WAVE TRANSMISSION PAST A FLOATING BREAKWATER WITH A PERFORATED FENCE

by

Ryan Patrick Mulligan

B.Sc.E., Queen's University, Kingston, 1997

A thesis submitted in partial fulfillment of the requirement for the degree of

Master of Applied Science

in

The Faculty of Graduate Studies

Department of Civil Engineering

We accept this thesis as conforming to the required standard

THE UNIVERSITY OF BRITISH COLUMBIA

September, 1999

In presenting this thesis in partial fulfilment of the requirements for an advanced degree at the University of British Columbia, I agree that the Library shall make it freely available for reference and study. I further agree that permission for extensive copying of this thesis for scholarly purposes may be granted by the head of my department or by his or her representatives. It is understood that copying or publication of this thesis for financial gain shall not be allowed without my written permission.

(Signature)

Department of CIVIL ENGINEERING

The University of British Columbia
Vancouver, Canada

Date September 29, 1999

DE-6 (2/88)

ABSTRACT

Floating breakwaters are used to attenuate wave action near shorelines and provide wave protection in marinas. Many different designs have been used. This thesis describes a field and numerical study of wave propagation past a particular floating breakwater design. The design corresponds to a pile restrained, concrete caisson, floating breakwater with a perforated fence. The floating breakwater has been installed at Ganges on Saltspring Island, British Columbia. Field tests were carried out to estimate the transmission characteristics of the breakwater by subjecting it to boat-generated waves with varying heights, periods and directions. Several phenomena that influence the wave transmission, including the boat-generated wave characteristics, reflected and evanescent waves and breakwater motions are addressed in the analysis.

The numerical model is based on two-dimensional linear wave diffraction theory. The model is used to evaluate the breakwater's wave transmission performance for varying breakwater dimensions, wave periods, wave directions, breakwater motions and damping coefficients. The suitability and performance of the design predicted by the field study and numerical analysis are assessed.

Of the parameters that were examined in the analysis of the floating breakwater the breakwater dimensions were determined to have the greatest effect on wave transmission, the degree of damping and breakwater motions both have a large influence on the results and the incident wave direction has a relatively small effect.

Overall, the breakwater performs well for low wave-energy environments or in environments where the wave climate is dominated by boat-generated waves. The vertical perforated fence attached to the concrete caisson extends the effective draft of the floating breakwater and has been shown to improve wave reflection and cause increased damping. Therefore, the fence decreases wave transmission past the floating breakwater.

Due to gaps in the pile wells, the breakwater may undergo some roll motions, and it tends to behave as freely floating for short period waves, in which case roll resonance can occur.

TABLE OF CONTENTS

LIST OF TABLES

LIST OF PHOTOGRAPHS

LIST OF FIGURES

LIST OF SYMBOLS

The following symbols are used in this thesis:

a	half the breakwater beam, B/2
A_n	complex coefficient
b	barrier thickness
B	breakwater beam, or width
c	wave celerity
c_{jk}	stiffness matrix
C	coefficient
C_m	added mass coefficient
C_t	wave transmission correction factor
d	water depth
dof	degrees of freedom
$F_j^{(e)}$	exciting force
g	gravitational constant
H	wave height
H_d	wave height measured on the downwave side
H_i	incident wave height
H_r	reflected wave height
H_t	transmitted wave height
H_u	wave height measured on the upwave side
i	$\sqrt{-1}$

k	wave number
ka	diffraction parameter, k times half the breakwater width
K_r	reflection coefficient
K_r'	apparent reflection coefficient (estimated from runup)
K_t	transmission coefficient
K_t'	apparent transmission coefficient (estimated from runup)
L	wavelength
m	wave mode order
m_{jk}	mass matrix
RAO	response amplitude operator
R_d	downwave runup
R_u	upwave runup
t	time
T	wave period
T_d	wave period measured on the downwave side
T_u	wave period measured on the upwave side
v_b	boat velocity
x	horizontal coordinate
y	horizontal coordinate orthogonal to x-direction
z	vertical coordinate or coordinate orthogonal to x-direction

α	incident wave angle (angle between the wave orthogonal and normal to the breakwater)
β	angle between the breakwater and wave orthogonal
Δ	angle between the breakwater orientation and boat direction
ϕ	velocity potential component
Φ	velocity potential
ϕ_j	forced wave potential
ϕ_s	scattered wave potential
ϕ_w	incident wave potential
λ_{jk}	damping matrix coefficient
μ_{jk}	added mass matrix coefficient
η_s	water surface elevation
θ	angle; angle between the boat direction and wave orthogonal
ω	angular wave frequency
∇	Laplacian operator
ξ	motion amplitude
ζ	damping coefficient

ACKNOWLEDGEMENT

The author would like to express his sincere appreciation and gratitude to his thesis advisor, Dr. Michael Isaacson, for his advice, support and guidance throughout this research. The author would also like to extend thanks to Mr. Ernie Watchorn, President and Chief Engineer of CeFer Floating Structures Ltd. for making the field tests possible.

Thanks also go to Nerissa Moscote and Gang Yang of the Department of Civil Engineering at University of British Columbia and Shea Watchorn of CeFer Floating Structures Ltd. for their field assistance.

Finally the author would like to thank his colleagues in Coastal and Ocean Engineering at UBC who have provided support and advice: Eric Morris, Premasiri Sundaralingam and John Baldwin. Finally, Nerissa Moscote deserves additional thanks for her limitless support.

1 INTRODUCTION

Society's increasing reliance on coastal resources for transportation, recreation and building materials has necessitated greater attention to the control of damaging wave action. Many structures have been developed to protect shores and control wave action along the coast. Thus, groins, jetties, seawalls and breakwaters are several types of coastal structures employed to protect beaches, marinas, inlets and coastal landforms. Breakwaters in particular are useful structures to attenuate waves and create calmer waters for boats and other structures.

1.1 FLOATING BREAKWATERS

The primary objective of any breakwater is to attenuate waves approaching a marina or shoreline. Breakwaters reduce wave heights by reflecting wave energy or dissipating wave energy. Many types of breakwaters have been built to control wave action, including both fixed and floating breakwaters. Fixed structures include rubblemound breakwaters and caisson-type breakwaters. Floating breakwaters can be much more attractive, both economically and environmentally, than conventional fixed structures. They are useful in deep water where a bottom-founded structure would result in very high material costs. Floating breakwaters differ from fixed breakwaters by allowing some wave energy transmission, sediment transport, water circulation and fish migration underneath the structure. However, the oscillatory motion of a floating structure in waves may limit the range of its applicability. Motions result when floating structures

are excited by the action of waves. Wave-excited structures must be designed such that the motion they experience is limited.

Floating breakwaters become ineffective if the wave height or wave period is too large. An important design parameter which influences the performance of a floating breakwater is the ratio of breakwater width B to wave length L. This ratio can also be expressed in terms of the diffraction parameter ka, where k is the wave number ($k = 2\pi/L$), a is half the width of the structure, and thus $ka = \pi B/L$.

Floating breakwaters have been designed in many different configurations and made from many different materials. Several common types of floating breakwater designs are shown in Fig. 1. Design choices include the number of pontoons or caissons, the shape of the cross-section of the structure, the mooring or restraint system and the construction material. Single pontoon, double pontoon and multi-pontoon or mat structures have been used. The cross-sectional geometry includes circular and rectangular sections and other irregular shapes. Materials used have included logs, treated wood, rubber tires, concrete, steel or composite materials. Restraint may be provided by fixed piles and cable mooring systems. Floating breakwater structural units and their mooring systems are vulnerable to failure during severe storms or failure due to fatigue from constant motion and impacting waves. For this reason, floating structures are subject to relatively high maintenance costs to keep them in place and functioning properly. Proper design of floating breakwaters is critical in ensuring good performance and extensive life.

A floating breakwater generally does not prevent all the incident wave energy from being transmitted. Thus, when an incident wave encounters a floating breakwater, some wave energy is reflected, some dissipated and some transmitted past the structure. For a floating breakwater to behave efficiently, most wave energy will be reflected or dissipated, and the resulting transmitted wave height H_t will be appreciably lower than the incident wave height H_i. The transmission coefficient K_t is defined as the ratio of transmitted wave height to incident wave height, $K_t = H_t/H_i$, such that a lower value of K_t indicates a more effective floating breakwater.

1.2 Literature Review

Aspects of the performance and design of floating breakwaters have been studied extensively. McCartney (1985), Werner (1988) and Cammaert *et al* (1994) have provided overviews of the knowledge of floating breakwaters, including their types, limitations and design considerations. Nece *et al* (1988) have summarized the successes and failures of several floating breakwater designs used in North America. Newman (1977), Sarpkaya and Isaacson (1981), Chakrabarti (1987) and Sawaragi (1995) have discussed the hydrodynamic analysis of floating bodies based on potential flow theory. Headland (1995) has summarized the mechanics and modeling of floating breakwaters.

Several researchers have extended hydrodynamic theory and have developed numerical models of floating breakwaters. Two-dimensional numerical models of floating breakwaters have been developed by Ito and Chiba (1972) and Adee and Martin (1974).

Ito and Chiba (1972) treated the problem by developing separate velocity potentials for interior and exterior hydrodynamic domains defined by the breakwater. Adee and Martin (1974) improved upon the method used by Ito and Chiba by allowing the evaluation of floating breakwaters of arbitrary shape. Isaacson and Nwogu (1987) have modeled a semi-immersed floating cylinder using the boundary element method. Their approach is discussed further in Chapter 4 and has been adopted as the numerical model for the present study. Brorsen and Bundgaard (1990) have also provided a numerical model based on the boundary element method. Their approach is used to calculate nonlinear lateral wave forces acting on large floating bodies.

Wave transmission past a floating breakwater has been studied both numerically and experimentally. Isaacson *et al* (1995) conducted experiments to model a circular-section floating breakwater. Isaacson, Baldwin and Bhat (1998) have examined wave propagation past a pile restrained floating breakwater. These studies compare numerical and experimental results and indicate excellent agreement. In general, field, laboratory and numerical tests have shown that floating breakwaters can be modeled with reasonable accuracy.

Gardner and Townend (1988) have reviewed studies on slotted vertical screen breakwaters and have provided comparisons between experimental and theoretically derived wave transmission coefficients for varying slot alignment and porosity.

1.3 Motivation for Study

The present study was prompted by interest in the evaluation of the performance of a new floating breakwater design. This breakwater, shown in Fig. 2, is comprised of a concrete caisson with a perforated vertical fence made from treated timber to reflect and dissipate wave energy. It was hypothesized that the addition of a gate with horizontal slots to the upwave side of the structure would decrease wave transmission, but the performance had not been quantified in the field. The present study was undertaken to assist CeFer Floating Structures Inc. in assessing the performance of the new design on the basis of both field tests and numerical modeling.

1.4 Objectives

The primary objective of this study is to determine the performance of a pile restrained, rectangular caisson floating breakwater with an attached perforated fence. The field tests were conducted to determine the performance of the floating breakwater at Ganges Harbour on Saltspring Island, British Columbia. The prototype structure was subjected to boat-generated waves of various heights, periods and directions, and transmission coefficients were determined from the tests.

The performance of the structure was also predicted by the use of a computer model. This enabled the effectiveness of the breakwater to be assessed over a wide range of conditions. The results of the field tests and the computer model are compared.

The study involves predictions based on both field tests and numerical modeling of the wave transmission past the breakwater subject to normal and oblique waves. The following summarizes the procedure followed to determine the performance and suitability of the Saltspring breakwater:

1. Field tests on the breakwater at Saltspring Island were conducted by measuring the wave height and period for waves generated from different boat speeds and directions. The breakwater motion was observed and reported on in qualitative terms. Chapter 2 provides a description of the site, the breakwater, the environmental conditions and the field tests.

2. Breakwater performance was analyzed by determining the wave transmission for each test. Results are provided in terms of the diffraction parameter ka and the transmission coefficient K_t for each incident wave direction. Results of the field tests and a discussion of the estimation of incident wave direction, wave period, transmission coefficient, breakwater motions, and measurement errors are presented in Chapter 3. In addition, error due to the influence of reflected and evanescent waves on the field measurements is estimated through a simple vertical barrier analysis and a corresponding correction factor is developed.

3. A computer model was used to estimate the transmission coefficient. Several rectangular breakwater dimensions were used to approximate the actual breakwater

geometry. For each case, different degrees of freedom of the breakwater were tested for various wave directions and damping coefficients: such that the structure is fixed, heave-only and freely floating. In Chapter 4, the numerical model description and methodology is introduced.

4. Results based on field performance and numerical predictions are compared. An analysis of the numerical model results is presented in Chapter 5. Field and numerical results of the floating breakwater performance are compared in Chapter 6. Finally, conclusions and recommendations are presented in Chapter 7.

2 FIELD TESTS

Ganges is the largest town on Saltspring Island, which is itself the largest of the Gulf Islands in Georgia Strait in southern British Columbia. The location of Saltspring Island and Ganges Harbour is shown in Figs. 3 and 4. The Ganges Harbour Sailing Club, where the breakwater under consideration is located, lies several hundred metres from the main boat channel. Since 1985, the sailing club marina has been protected by a series of log bundle breakwaters. This type of floating log structure is shown in Photo. 1 and can be found in use today in other areas of Ganges Harbour. A new floating breakwater, designed and installed by CeFer Concrete Floating Structures, was installed in February 1998 in an effort to reduce the effects of boat-generated waves on the sailboats and floating docks in the marina. In particular, the wakes of boats over 12 m in length were disturbing the sailing club. Photograph 2 shows the marina behind the new floating breakwater.

2.1 BREAKWATER DESCRIPTION AND DIMENSIONS

The floating breakwater, shown in Photo. 3, consists of two 40 m (130 ft) rectangular sections that are connected in series and run parallel to the shoreline. The marina lies between the breakwater and the shoreline. The structure also acts as a dock, with sailboats moored to the breakwater and the deck used for pedestrian access.

Six 0.4 m (16") diameter piles on the downwave side of the structure restrain the breakwater. The piles allow the breakwater to move vertically with the tide, but eliminate horizontal breakwater motions (surge and sway). Since 2.5 to 5.0 cm spaces exist in the pile wells, the breakwater may experience limited roll and pitch.

The breakwater includes vertical perforated fences made from treated wood on the upwave and downwave sides of the breakwater in order to reduce wave transmission. The breakwater geometry is rectangular and the structure is 3.96 m (13 ft) wide. The perforated timber fences extend 0.92 m (3 ft) below the 0.92 m thick foam filled concrete caisson. This is illustrated in a cross-section of the floating breakwater, shown in Fig. 2. The breakwater also includes water chambers behind the fences and relief holes in the deck. Photograph 4 shows the Saltspring breakwater and incident wave conditions. The effect of a large wave "spraying" through the relief holes on the breakwater deck can be seen in Photo. 5.

Tests were conducted on the breakwater over a period of two days, June 8 - 9, 1998. A 14 m boat, the CeFer Raider (see Photo. 6), was taken to the site and used to generate waves. The boat is powered by twin 260 HP engines and has a mass of approximately 12,700 kg (28,000 lb.).

2.2 FIELD TEST METHODOLOGY

The purpose of this study is to determine the performance of this breakwater configuration and validate this concept in floating breakwater design. The breakwater was subjected to boat-generated waves of various heights, periods and directions. Tests were conducted by varying the boat speed and direction with respect to the breakwater location. Boat speeds and directions were measured using the speedometer and compass aboard the vessel. Water depths at the breakwater were measured with a depth-sounder.

A simple apparatus was used to measure water surface elevations. A wooden bracket was placed around the third pile from the north end of the breakwater on the downwave side, as shown in Photos. 7 and 8. Since the pile did not experience any breakwater motion, the experimental set-up was immobile. This pile was not near the end of the breakwater so that diffraction effects did not significantly influence wave height measurements and no boats were docked close to this pile. As shown in Photo. 9, horizontal wooden beams extended from the bracket around the pile to plastic wave staffs. The beams extended 4.5 m to the wave staff on the upwave side of the breakwater and 1.5 m to the wave staff on the downwave side. Each staff was located 1.1 m away from the breakwater. Two video cameras were used to record water surface elevations at the wave staffs.

2.3 Environmental Conditions

Owens (1980) has conducted a shore-zone analysis of Saltspring Island for coastal planning. Saltspring Island has been described as a sheltered environment with low wave-energy levels at the shoreline. Owens reported that wave heights greater than 1.0 m are rare and are restricted to major storm events, but boat-generated waves regularly impact shores near harbours and channels. Since the island is surrounded by a series of interconnected channels, fetch lengths are very limited and thus storm surges are not usually important. Water-level changes due to wind generated effects are generally less than 0.5 m. The normal tidal range at Saltspring Island is 2 to 3 metres. The tides are described as mixed semi-diurnal with pronounced inequalities that often produce periods of "double" high tides (Owens, 1980). Strong tidal currents exist in the narrow channels surrounding the island.

The field tests began on June 8, 1998. The weather was sunny with a temperature of 20°C. A strong 25-30 km/h southeast wind blew into Ganges Harbour and created 0.3 to 0.6 m chop. These waves illustrated the performance of the breakwater under strong wind-generated waves, but complicated the testing by interfering with the boat-generated waves. During the tests the tide was high, with the water depth at the breakwater approximately 7.3 m (24 ft).

The tests were completed on June 9, 1998. The weather was cloudy with a temperature of 15°C. A light 8-15 km/h southeast wind generated waves less than 0.3 m in height.

The tide was intermediate during the tests, with the water depth at the breakwater approximately 5.8 m (19 ft).

On both days, wind-generated waves were observed to diffract around the breakwater ends. Boats behind the breakwater would sway gently in the presence of transmitted and diffracted wind-generated waves.

2.4 TEST CASES

Field tests were planned to cover a range of boat speeds and directions. Wave direction relative to boat direction and breakwater location is shown in Fig. 5. The boat was driven past the breakwater such that the angle between incident wave orthogonal and the normal to the breakwater ranged between 0 and 55 degrees. Therefore, several sets of oblique waves and normal waves would be used to test the breakwater. In addition, results were obtained by running the boat in the main channel further away from the breakwater. These tests simulated the speed, direction and distance of boat traffic in the main Ganges channel. For each direction, tests were repeated for several boat speeds, approximately 6.0, 7.5 and 9.0 m/s. This covered a wide range of directions and speeds. Due to unexpected wind and wave conditions at the site, several tests were discarded and several tests were repeated.

2.5 DATA ANALYSIS

Wave heights and periods were determined from the video records of the incident and transmitted waves. For the best three discernable boat waves for each test, the average wave height and period were determined. Slow motion tracking enabled the wave staffs to be read to an accuracy of ± 1 cm. The number of video frames per wavelength were counted to determine the wave periods with acceptable accuracy. Methods of estimating the ship-wave pattern, wave direction and wave period are discussed in this section.

2.5.1 Theoretical Ship-Wave Pattern

Understanding the wave pattern generated by a ship is important for determining the direction of the ship-generated waves. Figure 6 illustrates the theoretical pattern of wave crests generated by a ship. Newman (1977) has outlined the theory for ship-wave hydrodynamics whereby the free-wave distribution of a ship can be developed from a three-dimensional analysis of ship waves. The classical ship-wave pattern can be determined from the free-wave distribution. This ship-wave pattern, developed by Kelvin in 1887 is given by:

$$\frac{z}{x} = \frac{-\cos\theta \sin\theta}{1+\sin^2\theta} \qquad (2.1)$$

where x is the horizontal coordinate, z is the coordinate orthogonal to the x-direction and θ is the angle between the wave orthogonal and boat direction. It can be shown that Eq. 2.1 results in the theoretical ship-wave pattern shown in Fig. 6.

A ship generates two sets of waves: diverging waves and transverse waves. The diverging wave crests generated from the vessel are confined to a sector of $\pm$ 19°28' as indicated in Fig. 6. The angle between the wave orthogonal and boat direction lies in the range $35°16' < \theta < 90°00'$ for diverging waves. Therefore, diverging waves change in direction as they propagate away from the ship but reach a maximum of approximately $\theta = 35°$. Therefore the wave crests that intercept the floating breakwater change in direction and this change varies with time and with location along the length of the breakwater. The curvilinear pattern of diverging waves generated by the vessel used in the breakwater tests can be seen in Photos. 10 and 11.

2.5.2 Wave Direction Estimation

A diagram illustrating wave direction with respect to boat direction and breakwater orientation is presented in Fig. 5. For each test, the incident wave direction α, defined as the angle between the wave orthogonal and the normal to the breakwater, was estimated from the boat direction. Two methods were used. The first method uses the theory of ship-waves (e.g. Newman, 1977). The angle θ, between the wave orthogonal and the boat direction, is taken to have a value $\theta = 35°$. This angle applies to the portion of a wave crest that first reaches the breakwater (see Fig. 5). Therefore this angle was used to estimate the angle α between the wave orthogonal and normal to the breakwater. The breakwater azimuth of 280° and boat compass bearings were needed to carry out this calculation for each test.

The second method that was used to calculate the incident wave direction was based on the estimate of the wave celerity. Since deep water wave conditions were present, the wave celerity was determined from the wave period:

$$c = \frac{gT}{2\pi} \tag{2.2}$$

Since the waves were generated at an angle to the direction of velocity of the boat, the wave celerity and the boat velocity are related by:

$$c = v_b \cos\theta \tag{2.3}$$

where again θ is defined as the angle between the boat direction and the wave orthogonal. Therefore wave celerity c was calculated from the wave period and since the boat speed v_b is known, θ can be determined. Figure 5 illustrates the relationships between the direction of the boat, the breakwater orientation and the wave crests. To determine the incident angle α, the angle between the wave orthogonal and the normal to the breakwater, several other angles are needed: Δ is defined as the angle between the breakwater and boat direction, and β is defined as the angle between the breakwater and wave orthogonal. Therefore, in the first method, the angle between the direction of boat travel and direction of wave travel was assumed to be $\theta = 35^\circ$, while in the second method the angle θ was determined from the speed of the boat. Visual inspection during testing indicated that incident wave direction α in the tests ranged from $\alpha = 0^\circ$ up to about $\alpha = 50^\circ$.

Estimates of the incident wave direction α by both methods were in general agreement. The first method resulted in the incident wave direction ranging from $\alpha = 5^{\circ}$ to 55°; the second method yielded the range $\alpha = 3^{\circ}$ to 47°. In most cases the difference between the two predictions was less than 15°. In addition, the incident wave direction relative to the breakwater was estimated by eye, and these estimates generally agreed with the calculated wave directions.

2.5.3 Wave Period Estimation

The change in the ratio of the transmitted wave height to incident wave height with the change in wave period is used to determine the wave transmission past the floating breakwater. A reasonably accurate estimate of the wave period is vital to determining the wave transmission characteristics of the breakwater since the transmission coefficient depends strongly on the beam to wave length ratio. The wave period was estimated in three ways: from the measurements on the upwave side of the breakwater, and from calculations from the boat speed, and from the measurements on the downwave side of the breakwater.

In the first method, measurements taken on the upwave side of the breakwater were used to determine the wave period. The wave periods appeared to be very low and thus the ka values were generally very high. Several errors may have contributed to this, the primary

one being the superposition of wind generated, boat generated and reflected waves on the upwave side of the breakwater.

In the second method, the wave period was calculated from the velocity of the boat. The wave celerity, wave length and wave period were calculated based on the assumption that the angle between the direction of boat travel and wave orthogonal was $\theta = 35^{\circ}$. This relationship is illustrated in Fig. 5. This wave period calculated from boat velocity was on the order of 1 - 2 sec. longer than the wave period measured on the upwave side of the breakwater.

Finally, a third method was used to estimate the wave period. When the wave periods measured on the upwave and downwave sides were compared, it was noted that the downwave periods were longer and less variable. The upwave measurements are composed of a mixture of longer ship-generated waves and shorter wind-generated waves, resulting in a large variance in the wave period results. When wind-generated waves alone were present, wave transmission past the breakwater was negligible, whereas boat-generated waves were transmitted past the breakwater. Therefore the waves measured on the downwave side of the breakwater were thought to most closely represent the boat-generated wave period. Though the waves are attenuated in height, the downwave results provide the most accurate estimate of the boat-generated wave period.

3 FIELD RESULTS

The results of the field data analysis are presented in this charpter. Quantitative wave transmission results are presented and qualitative observations of breakwater motions are also considered. The data collected in the field is presented in Table 1. This data includes the wave periods and wave heights measured on the upwave and downwave sides of the breakwater, the water depth, the boat velocity and the boat direction. The wave data is presented in Fig. 7 through a comparison of incident wave heights to transmitted wave heights over a range of wave periods. This highlights the breakwater's capability of notably attenuating waves. The incident wave height and period is dependent on the boat velocity. A comparison of incident wave heights and periods for various boat speeds is shown in Fig. 8. In general a speed of 7.7 m/s (15 kts) generated the largest wave heights and periods.

3.1 WAVE TRANSMISSION RESULTS

On the basis of the discussion in section 2.5.3, wave periods based on the downwave measurements were used as a basis for determining the wave transmission results. Relevant wave transmission and wave direction results are provided in Table 2 and are presented in Fig. 9. The results range from approximately ka = 0.6 to ka = 1.7 and K_t = 0.15 to K_t = 0.95. The data appears to be quite scattered on this plot and therefore the relationship between wave transmission and wave direction should be considered.

The boat generated a variety of incident wave directions with which to test the floating breakwater. The data points obtained in the field tests are plotted for each wave angle are shown in Fig. 9, for the wave period determined from waves measured on the downwave side. This plot shows data with incident angles of 5°, 25°, 45° and 55°. Results for the same wave angle are not always consistent; however, as a general trend, obliquely incident waves result in lower transmission while normally incident waves cause greater wave transmission. This may be related to the breakwater motions since the breakwater configuration allows roll but limits pitch.

3.2 Effects of Breakwater Motion

In the field it was noted that roll motion increased for more normal waves (waves with smaller incident angles). When the incident wave angle was oblique, the incident waves encountered a greater effective breakwater width. Since the length of the breakwater is large relative to the wavelength, the breakwater did not experience pitch. When the incident angle was normal, the incident waves encountered a smaller effective breakwater width. The width of the structure is small relative to the wavelength and limited roll occurred.

The design of the breakwater allows its movement to be unlimited with respect to heave, since the structure must be able to move vertically, restrained by piles, following the large tidal range at the site. Although there was negligible heave arising from wind-generated

waves, in some tests using boat-generated waves heave motions were severe particularly when the boat was travelling at a high velocity very close to the structure.

It was also found that significant, but limited roll occurred for several tests - this being possible due to the presence of a gap between the piles and the guide timbers in the pile wells. Strong rolling action occurred when the largest waves encountered the structure from a direction normal to the breakwater.

A cross-section of a pile well is presented in Fig. 10, with no gaps indicated. However, the actual gaps between the piles and the pile wells were on the order of 2.5 to 5.0 cm. The maximum roll angles for different gap sizes were determined from geometric considerations as shown in Fig. 11. The relationship between maximum allowable roll angle and gap width is shown in Fig. 12. For a 5.0 cm gap, the maximum allowable roll angle is 17^{o}, while for a 2.5 cm gap the maximum roll is 10^{o}. This analysis was performed to determine if the gaps were large enough to allow roll to the full extent of predicted freely floating roll motion and is pursued further in Chapter 6 by comparing the physical roll limitations with the numerically predicted roll amplitude. However roll would not be perpetually limited because the guide timbers would begin to be crushed after several load cycles. Due to the restraint of the breakwater, the roll limitations would be removed after repeated roll action.

3.3 MEASUREMENT ERRORS

There are several errors involved with field data collection, which have caused some uncertainty in the results and must be addressed. A close-up view of the upwave staff, as shown in Photo. 9, allowed water levels to be read. However, the water level readings include reflected and wind-generated waves superimposed over the boat-generated waves and therefore affect the reading of the wave height and period. Since measurements were taken only 1 metre from the breakwater, reflection and evanescent modes would have influenced the results.

The wave staff could be read to an accuracy of ± 1 cm, but splash-up on the rod influenced the visibility of the scale. Ideally, the apparatus was held fixed, whereas some movement of the apparatus due to wave forces acting on the thin plastic wave staffs occurred and affected the results.

Wave periods and heights were determined from the video by averaging the measurements for three successive waves bearing in mind that since the waves are boat-generated, the wave period, wave height and wave direction changed with time. It is noted also that the data was measured at two points near the breakwater, and variation of wave height, period and direction along the breakwater's length was not considered.

The weather at the site, particularly on the first day of testing, was very windy. The wind blew directly onshore at the sailing club marina, as shown in Photo. 2. Wind-generated

waves combined with the boat-generated waves used in the tests. From the video analysis, wind-generated waves were estimated to be 3 - 4 cm in height in the absence of boat-generated waves on the downwave side and 10 - 15 cm in height on the upwave side. Therefore, wind-generated waves provided a contribution of 15% - 35% of the height of the measured waves on either the upwave or downwave side.

Since the wave staffs were used to measure the water surface elevation, the waves measured on the upwave side were combined incident and scattered waves. The incident waves were composed of mixed wind and boat-generated waves, previously discussed. The scattered waves were mixed reflected (propagating) and evanescent mode (decaying) waves. In the following section, a method for numerically estimating reflection and evanescence is described and is used to predict the influence of reflected and evanescent waves.

3.4 Vertical Barrier Analysis

The purpose of the following analysis is twofold: to show the effects of reflection and evanescence on the wave measurements and to develop a correction factor for the wave transmission field data.

One concern with the measurement method used here is that the wave staffs were relatively close to the breakwater, so that a correction is needed to account for reflected and evanescent waves on the upwave side and evanescent waves of the downwave side.

Evanescent mode waves are scattered waves that decay with distance from the structure. Since wavelengths were generally on the order of 20 to 30 metres, and wave measurements were taken 1 metre away from the breakwater, evanescent waves would not have decayed and were expected to contaminate wave height measurements. In order to estimate these effects, the breakwater is simplified as a thin vertical barrier, corresponding to the timber fence. An approximation for numerically estimating the influence of reflected and evanescent waves is described. This is achieved by comparing an apparent transmission coefficient based on the wave runup on the upwave and downwave sides of the barrier, which is what the wave staffs actually measure, with the theoretical transmission coefficient.

The influence of reflected and evanescent waves can be estimated numerically by considering the reference case of a vertical barrier (Yang, 1996). The model is based on the eigenfunction expansion method and the breakwater is simplified to a single, thin vertical barrier. The fluid is divided into two regions corresponding to the upwave and downwave sides of the structure.

To evaluate the influence of reflected and evanescent waves, the reflection coefficient, K_r, can be evaluated far from and close to the structure for normally incident waves. The scattered wave potential upwave of the structure ($x < 0$) can be expressed as:

$$\Phi_s = -C\left[A_o \cosh(k_o s)\exp(-ik_o x) + \sum_{n=1}^{\infty} A_n \cos(k_n s)\exp(k_n x)\right]\exp(-i\omega t) \qquad (3.1)$$

where

$$C = -\frac{igH}{2\omega}\frac{1}{\cosh(k_o d)} \tag{3.2}$$

and H is the incident wave height, g is the gravitational constant, k_o is the wave number, x is the horizontal coordinate, ω is the wave frequency, $i = \sqrt{-1}$ and A_n are complex coefficients that can be evaluated numerically. Since only propagating wave modes (m = 0) exist at locations far from the structure,

$$\Phi_s = -C[A_o \cosh(k_o s)\exp(-ik_o x)]\exp(-i\omega t) \qquad \text{for } x \to -\infty \tag{3.3}$$

Using the scattered wave potential to solve for the corresponding component of the water surface elevation gives:

$$\eta_s = \frac{H}{2} A_o \exp[-i(k_o x + \omega t)] \tag{3.4}$$

The reflection coefficient can be calculated from the amplitude of the water surface elevation:

$$K_r = \left|\frac{H_r}{H}\right| = |A_o| \tag{3.5}$$

This estimate of the reflection coefficient is made at a distance far from the structure where evanescent modes have decayed. The reflection coefficient can also be estimated from runup at the structure where evanescent modes have not decayed. The runup can be

evaluated from the total velocity potential when x = 0. The runup on the upwave side of the structure is the sum of the incident, reflected and evanescent wave components:

$$R_u = \frac{H}{2}\left|1 - A_o - \frac{1}{\cosh(k_o d)} \sum_{n=1}^{\infty} A_n \cos(k_n d)\right| \tag{3.6}$$

The apparent reflection coefficient, estimated at the structure, is therefore:

$$K_r' = \frac{2R_u}{H} - 1 \tag{3.7}$$

where the incident wave height H has been subtracted to isolate the reflected wave height $2R_u$. A comparison of these two methods illustrates the difference in scattered wave height close to and far from the barrier, the difference being the presence of evanescent mode waves close to the structure. For a solid vertical barrier with the depth and draft conditions of the Saltspring breakwater the results are shown in Fig. 13. The vertical distance between the curves represents the influence of evanescent modes for a given wave period. The figure clearly shows how the apparent reflection coefficients, estimated on the basis of wave measurements at the barrier, are higher than the true reflection coefficients.

Evanescent waves contribute approximately 20% of the reflected wave height to the measurements taken close to the structure. Reflected waves undoubtedly have influenced the field measurements but the effect of evanescent waves is minimal.

Similarly, for conditions downwave of the barrier ($x \rightarrow \infty$), the transmission coefficient can be developed. Far from the structure:

$$K_t = |1 + A_o| \tag{3.8}$$

At the barrier, the downwave runup is:

$$R_d = \frac{H}{2}\left|1 + A_o + \frac{1}{\cosh(k_o d)} \sum_{n=1}^{\infty} A_n \cos(k_n d)\right| \tag{3.9}$$

Therefore the apparent transmission coefficient based on elevations estimated at the barrier is:

$$K_t' = \frac{R_d}{R_u} \tag{3.10}$$

The relationship between K_t and K_t' is shown in Fig. 14. The transmission estimated from the runup at the barrier is approximately 10% greater than the true transmission coefficient.

3.4.1 Development of a Wave Transmission Correction Factor

In order to estimate and filter out the effects of reflected and evanescent waves from the field measurements, a correction factor has been developed and applied to the field data. This wave transmission correction factor C_t is shown in Fig. 15 and was developed from

the aforementioned single vertical barrier analysis. The correction factor is the ratio between the transmission coefficient K_t and the apparent transmission coefficient K_t':

$$C_t = \frac{K_t}{K_t'} \tag{3.11}$$

From field measurements of downwave and upwave runup, the apparent transmission coefficient K_t' was estimated for each test. When the transmission correction factor C_t is multiplied by K_t' obtained from the field measurements, the result is the transmission coefficient K_t, corrected for reflected and evanescent waves. Corrected and uncorrected field data is displayed in Table 3 for comparison. The corrected K_t is larger than the uncorrected K_t' as shown in Fig. 16 since the incident wave height has been reduced because reflected waves have been eliminated.

4 NUMERICAL TESTS

Apart from the field tests, a numerical approach was also used to evaluate the performance of the Saltspring floating breakwater, and this is described in this section.

4.1 NUMERICAL MODEL

The following is a discussion of the theory and assumptions made in the numerical analysis of a floating breakwater. The theoretical approach, after Sarpkaya and Isaacson (1981), analyses the fluid flow by applying the appropriate governing equations on the basis of linearized potential theory and expresses the flow in terms of a superposition of incident, scattered and forced waves. The boundary element method is used to solve for the velocity potential and the reflection and transmission coefficients can thereby be obtained (Isaacson and Nwogu, 1987).

4.1.1 Fluid Motion and Boundary Conditions

The fluid is assumed to be incompressible and inviscid and the flow is assumed to be irrotational so that the fluid motion can be expressed in terms of a velocity potential, Φ which satisfies the Laplace equation:

$$\nabla^2\Phi = \frac{\partial^2\Phi}{\partial x^2} + \frac{\partial^2\Phi}{\partial y^2} + \frac{\partial^2\Phi}{\partial z^2} = 0 \qquad (4.1)$$

Several boundary conditions are needed to define the problem. These include conditions at the seabed, the free surface, the structure surface and radiation boundaries. From these conditions the linear dispersion relation, relating the wave frequency to wave number, can be established:

$$\omega^2 = gk \tanh(kd) \tag{4.2}$$

where ω is the wave frequency, g is the gravitational constant, k is the wave number and d is the water depth. When there is no structure present, a solution for a regular wave train leads to an expression for the incident velocity potential:

$$\Phi = \frac{\pi H}{kT} \frac{\cosh(k(z+d))}{\cosh(kd)} \sin\theta \tag{4.3}$$

where $\theta = kx - \omega t$ is the wave phase angle, H is the wave height and T is the wave period.

A floating body, such as a floating breakwater or ship, is subject to movement with several degrees of freedom. The body's motion can be related to the velocity potential through the fluid force acting on the body and the equations of motion of the system. A rigid floating body may experience motions with six degrees of freedom as indicated in Fig. 17: three translational motions (surge, sway and heave) and three rotational motions (roll, pitch and yaw). Each component motion gives rise to a set of forced waves described by a potential $\Phi_j^{(f)}$. Thus the total velocity potential Φ can be expressed as a linear superposition of three potentials:

$$\Phi = \Phi_w + \Phi_s + \sum_{j=1}^{6} \Phi_j^{(f)} \tag{4.4}$$

where subscripts w and s refer to the incident and scattered wave fields respectively and $\Phi_j^{(f)}$ represents each potential component associated with forced waves due to the motions of the body. The total velocity potential can be expressed in complex form as:

$$\Phi = \left[\frac{-i\omega H}{2} (\phi_s + \phi_w) + \sum_{j=1}^{6} -i\omega \xi_j \phi_j \right] \exp(-i\omega t) \qquad (4.5)$$

where ϕ_j refers to the forced wave potentials that correspond with each mode of motion, ξ_j is the motion amplitude in the j-th mode of motion, ω is the wave frequency and $i = \sqrt{-1}$. The equations of motion of a six-degree of freedom system can be expressed in the form:

$$\sum_{k=1}^{6} \left[-\omega^2 (m_{jk} + \mu_{jk}) - i\omega \lambda_{jk} + c_{jk} \right] \xi_k = F_j^{(e)} \qquad (4.6)$$

where m_{jk} and c_{jk} refer to matrices of mass and stiffness; μ_{jk} and λ_{jk} are added masses and damping coefficients which are associated with the forced potentials ϕ_j; and $F_j^{(e)}$ is the exciting force associated with $\phi_w + \phi_s$. In the case of a pile restrained floating breakwater, motions are confined to heave only and the equations of motion are simplified.

4.1.2 Numerical Solution

A boundary element method can be used to solve for the velocity potential (e.g. Isaacson and Nwogu, 1987). Following the determination of velocity potentials over the surface of the breakwater, the hydrodynamic coefficients (added masses, damping coefficients and exciting forces) may be obtained. The equations of motion may then be solved to obtain the breakwater

motions. Finally, the transmission coefficient K_t and reflection coefficient K_r are determined from the velocity potentials and breakwater motions.

4.2 Numerical Methodology

A computer model HAFB (Hydrodynamic Analysis of a Floating Breakwater) has been used to compute numerical results for the problem at hand. This model uses linear potential theory to predict wave loads and motions of an infinitely long, floating body of arbitrary shape subjected to a regular oblique wave train (Nwogu, 1985). The boundary element method is applied to formulate the problem in terms of a distribution of sources around the structure, the free surface and radiation boundaries or the upwave and downwave sides of the breakwater.

The numerical model was used to test the characteristics of a floating breakwater. The model was used to evaluate the performance of an existing breakwater by testing the effect of different breakwater dimensions, wave directions, damping and breakwater motions on wave transmission over a range of wave conditions. The breakwater analysis was conducted using HAFB with the breakwater configuration idealized as rectangular.

4.3 Test Cases

Two cases with different breakwater dimensions were used to simulate the Saltspring breakwater design as shown in Fig. 18. In both cases, the breakwater section geometry was specified to be rectangular. In case 1, a rectangular breakwater without the fence was used. In

case 2, a rectangular breakwater with a draft corresponding to the fence extension was used. This is equivalent to the assumption that the water between the two fences was considered to move in unison with the breakwater. With the fence in place, case 2 has a greater height, draft, cross-sectional area, moment of inertia and radius of gyration than the case 1 configuration. Since the addition of the fence extension to case 2 did not result in an increase in mass of the breakwater, both cases have equal centres of buoyancy and centres of gravity. For all numerical tests, the water depth was assumed to be 5.8 m. Table 4 lists the relevant input data for each case.

There are several parameters in addition to the breakwater geometry, which influence the performance of the breakwater: incident wave angle, degrees of freedom of motion, and the extent of hydrodynamic damping. For each case, these parameters were varied and the resulting breakwater performance was evaluated. The incident wave direction was set at $\alpha = 0^{o}$, 25^{o}, 35^{o} and 55^{o} so that the range of incident wave directions experienced during the field tests were simulated and effect of normal and obliquely incident waves were compared. The stiffness matrix was also varied allowing the breakwater to behave as if fixed, to move with respect to heave only, or move as if freely floating. This allowed an evaluation of the influence of the motion of the breakwater, since field observations noted limited roll due to the gap between the piles and pile wells. In addition, varying damping coefficients were used to help simulate the effect of the perforated timber fence. The water chambers and fence may act as dampers of the wave transmission on the otherwise rectangular structure. To test the effect of damping, damping coefficients of $\zeta = 0\%$, 5%, 10% and 15% were used.

5 NUMERICAL RESULTS

In order to assess numerically the influence of the performance of the Saltspring floating breakwater, several parameters have been examined: these include the breakwater dimensions, the incident wave direction, the magnitude of hydrodynamic damping and alternate constraints on the breakwater motions. The influence of each of these variables on breakwater performance is assessed by evaluating the transmission coefficient as a function of the diffraction parameter, ka.

5.1 BREAKWATER DIMENSIONS

Cases 1 and 2, described in chapter 4, were used to simulate the geometry of the Saltspring structure and the predicted variation of K_t vs. ka for both cases is shown in Fig. 19. It is seen that the responses for the two cases differ mainly in the region $1 < ka < 2$. As expected, the transmission is greater for case 1 than case 2 because of the shallower draft. For small values of ka, the breakwater is not effective and wave transmission is near 100% for both cases. For high values of ka, the waves have short wave lengths relative to the width of the structure and therefore both cases, having equal width, show excellent wave attenuation, with $K_t \approx 0.1$ for $ka > 2$.

5.2 Wave Direction

The breakwater performance for incident wave angles α = 0, 25, 35 and 55 degrees were tested using the numerical model and the corresponding results for a fixed breakwater are shown in Fig. 20. It can be seen that the incident angle is predicted to have a small effect on the wave transmission of the floating breakwater. Larger changes can be seen between normally incident waves (0-10°) and obliquely incident waves (45-55°), such that a larger, more oblique incident wave angle results in lower wave transmission. Figure 21 illustrates corresponding results for the case of a breakwater restrained to heave motions only. Again wave direction is seen to have a small influence on wave transmission.

5.3 Damping

The effect of varying the damping coefficient on the transmission coefficient is illustrated in Fig. 22 for the case 1 breakwater with damping coefficients ζ = 0, 5, 10 and 15% used. As expected, the results illustrate how increased damping results in a decrease in wave transmission.

As shown in Fig. 22, a large peak occurs for the freely floating breakwater for case 1 when ka = 2.8, corresponding to a wave period of 1.69 sec. The hydrodynamic analysis also provides the natural periods of the breakwater in heave and roll and predicts these to be approximately 2.8 sec. for heave and approximately 1.7 sec. for roll. Therefore the

freely floating breakwater is seen to experience resonance in roll when T = 1.7 sec. (ka = 2.8). The resonant effect is clearly less prominent when the value of the damping coefficient is increased.

The transmission coefficient as a function of ka for various damping coefficients for the case 2 breakwater dimensions are shown in Fig. 23. The roll resonance peak occurs at a lower value of ka than the first case, and as before increased damping reduces this peak significantly.

5.4 Breakwater Motions

Three cases of breakwater restraint were evaluated. Results have been obtained by changing the stiffness matrix in the equations of motion such that the breakwater would behave as (i) fixed, (ii) freely floating or (iii) restricted to heave-only. Figure 24 shows the wave transmission resulting from the three types of breakwater motions for the case 1 breakwater dimensions, normally incident waves and zero damping. When the breakwater is freely floating, resonance in roll can result, whereas when the breakwater is confined to heave-only motions, no resonant peaks result. The fixed breakwater clearly is the most effective for wave attenuation. For ka < 2, the freely floating and heave-only results are comparable. For ka > 2, fixed and heave-only models perform similarly. Therefore motion with respect to heave approximates the response of the fixed structure for high ka and is closer to the response of the freely floating breakwater for low ka. This

finding is intuitive since the heave-only breakwater does not experience the roll of the freely floating structure for high values of ka.

It should also be noted that roll resonance for the freely floating structure in case 1 differs from case 2. In case 1, roll resonance occurs when T = 1.7 sec. (ka = 2.8). Figure 25 illustrates the effect of changing the allowable breakwater motions for case 2. For case 2, the natural period for roll occurs when T is 2.2 sec. and for heave when T is 3.6 sec. The resonant peak occurs in roll when T = 2.2 sec. (ka = 1.6). The resonant peaks are very different depending on the geometry of the breakwater, but for fixed breakwaters, both cases behave very similarly.

5.5 Discussion

The above summary of the effect of changing individual variables is a useful first step in determining the behaviour of the floating breakwater. But in assessing the performance of the actual structure, simultaneous changes in these parameters need to be considered.

The effect of the change in breakwater geometry was evaluated for case 1 and case 2. Case 2 is intended to provide a means of accounting for the presence of the timber fence. However, the addition of the fence can also be viewed as providing additional "dampers" to the system, since the mass is not increased but wave attenuation increases. A comparison between case 1 with damping and case 2 without damping is shown in Fig.

26. With an increase in the value of the damping coefficient, the wave transmission in case 1 comes closer to the results of the undamped case 2.

The breakwater motions can vary for different wave periods, depending of the physical restraint on the structure. The breakwater behaves as freely floating for high values of ka, when the wave period is short, possibly leading to resonance, and as heave-only for low values of ka, when the period is long. This behaviour results because the maximum roll is reached in long waves so that the breakwater is then limited to heave-only motion, while in short waves the breakwater roll is less than the maximum allowable roll so that the breakwater behaves as freely floating. During some of the field tests, severe roll was noted, with abrasion between the piles and pile wells occurring. When the waves are longer, the amount of roll is limited due to the relatively small gaps between the piles and the structure. The breakwater behaves as heave-only in long waves since the breakwater is restricted from moving in all other directions.

6 COMPARISON OF FIELD AND NUMERICAL RESULTS

To compare field test results and computer model results, field and numerical data have been plotted together to illustrate several important trends.

6.1 PERFORMANCE OF THE SALTSPRING BREAKWATER

Dimensions and cross-sectional geometry play a major role in the performance of the floating breakwater. The field data and the numerical results for different breakwater dimensions are shown in Fig. 27 with the numerical results corresponding to zero damping, normally incident waves and heave-only motions. The numerical results for case 2 are similar to the field test results. Therefore, the addition of the fence to the structure is beneficial. Wave transmission decreases when the draft is increased. Since the fence extends the draft of the structure, this is an economical way of increasing the effective draft without building a larger concrete caisson.

The allowable breakwater motions also greatly effects its performance. Figures 28 and 29 show responses for fixed, heave-only and freely floating motion for the first case and the second case of breakwater dimensions respectively. The results shown in Fig. 29 support the hypothesis that the breakwater behaves as heave-only for values of low ka (high T) since the breakwater is restricted from movement in all directions except the vertical direction by the piles. The breakwater behaves as freely floating for values of higher ka (lower T) since the gaps between the piles and the guide timbers in the pile wells allow roll to occur. When the wave length is shorter, the breakwater is excited to

roll up to an amount less than the maximum allowable roll. Therefore the breakwater can experience resonance in roll. This can be seen in Fig. 29, with excellent correlation between field data and numerical results.

The amplitude of roll motion was numerically predicted. The response amplitude operator (RAO) in roll was determined for each breakwater test case. The RAO in roll is given by:

$$RAO_{roll} = \frac{\xi_r B}{H/2} \tag{6.1}$$

where ξ_r is the amplitude of roll motion in radians, B is the breakwater beam and H is the incident wave height.

For case 1 breakwater dimensions, roll resonance occurred when T = 1.7 sec. (ka = 2.8). The RAO in roll was determined to be 3.36 at the resonance peak. A wave with a period of 1.7 sec. was estimated to have a maximum incident height of 0.30 m from the field test results and the roll angle was determined to be 7.3°. For this case, the predicted roll does not reach the limiting angles of 10° or 17° imposed by the guide timbers in the pile wells around the piles for either a 2.5 or 5.0 cm gap respectively (see Fig. 12). The breakwater is therefore unlimited in roll and resonance can be reached. For the case 2 breakwater dimensions, roll resonance occurred when T = 2.2 sec. (ka = 1.6). The RAO in roll was determined to be 4.84 at the resonant peak. A wave with a period of 2.2 sec. was estimated to have a maximum incident height of 0.45 m from the field test results and the roll angle was determined to be 15.8°. Therefore the predicted roll does not reach the

limiting angle of 17° imposed by the pile wells around the piles for the 5.0 cm gap, but exceeds the maximum angle of 10° for the 2.5 cm gap. In this case, it is likely that significant roll could occur since the corners of the guide timbers would be crushed after several load cycles, effectively increasing the size of the gap. The boat-generated waves, measured downwave of the breakwater, range in period from 2.0 to 3.5 sec. This range contains the predicted resonance peak period and therefore it is likely that the breakwater could experience waves that excite the structure to resonance.

Therefore the numerical results indicate that the extent of the roll of the structure is close to if not less than the maximum possible roll. Only in cases of higher and longer waves or smaller gaps will the breakwater be fully limited for motion with respect to roll.

The wave direction also affects wave transmission past the floating breakwater. The field and numerical results for high and low incident wave directions are shown in Fig. 30 and a general trend is present. A smaller wave angle α, or a more normally incident wave direction, results in greater wave transmission. A larger, more oblique wave direction causes lower wave transmission. This is because as the incident wave direction increases, the effective width of the breakwater increases and smaller transmitted waves result.

The level of hydrodynamic damping in the computer model also affects the predicted breakwater performance. Applying a higher damping coefficient can bring the numerical results closer to the measured results. In this way, damping can be used in the numerical

model to simulate the damping effect of the fence attached to the breakwater. This can be done to simulate the effect of the actual damping caused by the breakwater. The field results and numerical results for different damping coefficients for the case 1 dimensions are shown in Fig. 31 and the results for the case 2 dimensions are indicated in Fig. 32. A greater damping coefficient in the numerical analysis reduces the wave transmission and simulates the field data with better accuracy.

7 CONCLUSIONS AND RECOMMENDATIONS

Field and numerical model tests were carried out to determine the performance of a floating breakwater at Ganges, Saltspring Island. In the field tests, the breakwater was subjected to boat-generated waves of varying direction, height and period. In the numerical tests, the influence of wave direction, breakwater motions, damping, breakwater dimensions, and wave period were examined. Overall, the breakwater performs well for the wave climate at Ganges. The perforated vertical fence attached to the floating concrete rectangular caisson extends the effective draft of the structure, increases wave reflection, and also causes increased damping. Therefore, the fence decreases wave transmission past the floating breakwater.

The field tests were conducted using a simple method of measuring waves with wave staffs and video recorders. The method was effective due to its simplicity and short set-up time. However, more accurate wave records would aid the accuracy of the results. Wave reflection and wind-generated waves contaminated the upwave measurements and complicated the tests. Downwave measurements were not affected by wind waves or reflected waves, and therefore the downwave record was used to determine the wave period. A simple vertical barrier analysis has shown that reflected waves influence the upwave measurements significantly, but that evanescent waves have a relatively small effect: they are less than 20% of the reflected wave height; and on the downwave side evanescent waves contribute less than 10% to the transmitted wave height. A correction

factor has been developed from the analysis and applied to the field data to correct for reflected and evanescent waves.

A comparison between the results of field tests and numerical model tests has revealed several major findings. Firstly, the perforated fence is beneficial to lower wave transmission. Since the fence effectively increases the draft of the floating structure, breakwater dimensions are a large factor. Varying the fence depth and permeability were not tested but are important parameters in determining how much wave energy is reflected, dissipated and transmitted past the breakwater.

Secondly, the breakwater can experience roll. It was initially assumed that the breakwater was allowed to move in the direction of heave only. This assumption was not valid. The breakwater is also allowed to roll due to the gaps between the piles and the guide timbers in the pile wells. The breakwater behaves as freely floating for high values of ka, in which case roll resonance can occur.

Of the parameters that were examined in the analysis of the floating breakwater, the breakwater dimensions were determined to have the greatest effect on the wave transmission performance of the structure, the degree of damping and degrees of freedom of motion both have a large influence on the results and the incident wave direction has a relatively small effect.

Field tests at the breakwater site were limited by the short range of wave periods generated by the boat. One recommendation for future design work on this breakwater would include performing physical model tests. This could allow a greater range of wave periods, wave heights and wave directions to be generated. Another recommendation is to design better restraint of the breakwater around the piles. The breakwater experienced roll motion due to the gaps in the pile wells, which occurred in the range of roll resonance. To minimize rolling motions and reduce wave forces, an improved bracket should be designed to restrain the breakwater.

The breakwater design used at Saltspring Island could be applied to other sites. The breakwater performs well for low wave energy environments or in environments where the wave climate is dominated by boat-generated waves. These conditions may exist in other locations in the Gulf Islands in South Western British Columbia, protected coastal areas or lakes. The breakwater is clearly useful for marinas or shore protection. However, the wave climate and conditions must be assessed before the same structure could be used again. Additional testing and possibly re-design would be necessary for higher wave energy environments. Physical modeling for this breakwater configuration could extend the analysis of this design and would be the logical next step in determining the performance of the breakwater for more severe wave conditions.

8 REFERENCES

Adee, B.H. and Martin, W., 1974. Theoretical Analysis of Floating Breakwater Performance, *Proceedings of the Floating Breakwater Conference*, University of Rhode Island, Kingston, Rhode Island, pp. 21-40.

Brorsen, M. and Bundgaard, H., 1990. Numerical Model of the Nonlinear interaction of Waves and Floating Bodies, *Coastal Engineering,* pp. 3140-3151.

Byres, R., 1988. The Application of Floating Breakwaters in British Columbia. M.A.Sc. Thesis, The University of British Columbia.

Cammaert, A.B., Morey, B., Lesley, L. and Warren, T., 1994. The Development of a Design Manual for Floating Breakwaters in the Atlantic Environment. *Ocean Engineering Resources Centre*, Memorial University of Newfoundland, Report No. TR-FIS-94002.

Chakrabarti, S.K., 1987. HYDRODYNAMICS OF OFFSHORE STRUCTURES. Computational Mechanics Publications, Southampton, England.

Dean, R. and Dalrymple, R., 1984. WATER WAVE MECHANICS FOR ENGINEERS AND SCIENTISTS. Prentice-Hall Inc., New Jersey.

Garceau, N., 1997. Combined Transmission and Diffraction Around a Floating Breakwater. M.A.Sc. Thesis, The University of British Columbia.

Gardner, J. and Townend, I., 1988. Slotted Vertical Screen Breakwaters. *Design of Breakwaters: Proceedings of the Conference Breakwaters '88*, Thomas Telford Limited, London, pp. 283–298.

Headland, J.R., 1995. Floating Breakwaters. In MARINE STRUCTURES ENGINEERING: SPECIALIZED APPLICATIONS, G.P. Tsinker (ed).

Isaacson, M., 1993. Wave Effects on Floating Breakwaters. *Proceedings of the Canadian Coastal Conference*, Vancouver, Canada. Vol. 1, pp. 53-66.

Isaacson, M., 1993. Users Guide to the Program HAFB: Hydrodynamic Analysis of a Floating Breakwater, The University of British Columbia.

Isaacson, M., Baldwin, J. and Bhat, S., 1998. Wave Propagation Past a Pile-Restrained Floating Breakwater, *International Journal of Offshore and Polar Engineering*, Vol. 8, No. 4, pp. 265-269.

Isaacson, M. and Nwogu, O., 1987. Wave Loads and Motions of Long Structures in Directional Seas, *Journal of Offshore Mechanics and Arctic Engineering*, Vol. 109, pp. 126-132.

Isaacson, M., Premasiri, S. and Yang, G., 1998. Wave Interactions with Vertical Slotted Barrier, *Journal of Waterway, Port, Coastal and Ocean Engineering*, Vol. 124, No. 3, pp. 118-126.

Ito, Y. and Chiba, S., 1972. An Approximate Theory of Floating Breakwaters, *Report of the Port and Harbor Research Institute*, Ministry of Transport, Japan, Vol. 11, No. 2, pp. 138-213.

McCartney, B.L., 1985. Floating Breakwater Design, *Journal of Waterway, Port, Coastal and Ocean Engineering*, Vol. 111, No. 2, pp. 304-318.

Nece, R., Nelson, E. and Bishop, C., 1988. Some North American Experiences with Floating Breakwaters. *Design of Breakwaters: Proceedings of the Conference Breakwaters '88*, Thomas Telford Limited, London, pp. 299-312.

Newman, J., 1977. MARINE HYDRODYNAMICS. The MIT Press, Cambridge, Massachusetts.

Nwogu, O., 1985. Wave Loads and Motions of Long Structures in Directional Seas. M.A.Sc. Thesis, The University of British Columbia.

Owens, E.H., 1980. Physical Shore-Zone Analysis, Saltspring Island, BC. Woodward-Clyde Consultants, Victoria.

Pilkey, W.D. and Pilkey, O.H., 1974. MECHANICS OF SOLIDS. Quantum Publishers, Inc., New York.

Sarpkaya, T. and Isaacson, M., 1981. MECHANICS OF WAVE FORCES ON OFFSHORE STRUCTURES. Van Nostrand Reinhold Company, New York.

Sawaragi, T., 1995. COASTAL ENGINEERING – WAVES, BEACHES, WAVE-STRUCTURE INTERACTIONS. Elsevier Science B.V., Amsterdam.

Sorensen, R.M., 1978. BASIC COASTAL ENGINEERING. John Wiley and Sons, New York.

U.S. Army Corps of Engineers, 1984. SHORE PROTECTION MANUAL, 4th edition. U.S. Government Printing Office, Washington, D.C.

Werner, G., 1988. Experiences with Floating Breakwaters, a Literature Review. *Bulletin of the Permanent International Association of Navigational Congresses*, No. 63, pp. 23-30.

Whiteside, W.N., 1994. Performance of a Circular Cross-Section Moored Floating Breakwater. M.A.Sc. Thesis, The University of British Columbia.

Yang, G., 1996. Numerical Model of Wave Effects on Permeable Vertical Barriers Above the Seabed. M.A.Sc. Thesis, The University of British Columbia.

Tables

Test	T_u (s)	H_u (cm)	T_d (s)	H_d (cm)	d (m)	v_b (m/s)	boat direction (deg)
1	1.8	36.7	2.4	12.0	5.8	6.2	220
2	2.3	42.5	2.8	14.3	5.8	7.7	220
3*					5.8	9.3	220
4*	1.3	23.5			5.8	6.2	220
5	1.7	26.7	2.3	8.7	5.8	7.7	220
6	2.0	30.0	2.8	11.0	5.8	7.7	220
7	2.0	18.8	2.7	14.0	5.8	7.7	220
8	1.1	15.0	2.8	14.0	5.8	9.3	220
9	1.6	23.3	2.8	8.0	5.8	6.2	150
10	1.4	21.0	3.6	16.3	5.8	7.7	150
11	1.4	15.0	2.2	6.5	5.8	9.3	110
12	1.7	12.3	2.2	4.0	7.3	6.2	220
13*					7.3	7.7	220
14	3.2	26.0	2.6	10.3	7.3	7.7	220
15*					7.3	6.2	280
16	2.2	36.7	3.3	6.0	7.3	7.7	280
17	2.6	25.0	3.4	5.7	7.3	9.3	280
18	2.2	43.3	3.1	7.0	7.3	7.7	100
19a	2.1	21.0	3.6	6.3	7.3	7.7	280
19b*	1.4	14.0			7.3	7.7	100
20	1.4	11.3	2.9	3.5	7.3	9.3	100
21	1.9	30.0	2.5	5.0	7.3	7.7	100
22*	0.8	9.3			7.3	6.2	100
23	1.9	25.7	2.9	11.7	7.3	6.2	220
24	2.1	25.0	3.4	19.3	7.3	7.7	220
25	2.6	45.0	3.4	6.5	7.3	6.2	130
26	1.4	23.0	3.0	12.3	7.3	7.7	130
27*					7.3	7.7	130

* data not analyzed

Table 1: Field test data summary including the upwave and downwave measured wave height and period, water depth, boat velocity and boat direction for each test.

Test	K_t	α (deg) *1	α (deg) *2	ka *3	ka *4	ka *5
25	0.14	5	11	1.20	0.76	0.68
26	0.54	5	13	3.82	0.49	0.89
9	0.34	15	26	3.07	0.76	0.99
10	0.78	15	34	4.20	0.49	0.61
1	0.33	25	32	2.37	0.76	1.37
2	0.34	25	33	1.58	0.49	1.03
5	0.33	25	40	2.87	0.49	1.57
6	0.37	25	36	1.99	0.49	1.04
11	0.43	25	4	4.13	0.34	1.70
12	0.32	25	35	2.87	0.76	1.70
14	0.40	25	20	0.80	0.49	1.18
23	0.45	25	31	2.24	0.76	1.06
7	0.75	25	37	2.08	0.49	0.99
8	0.93	25	50	7.16	0.34	0.69
24	0.77	25	35	1.89	0.49	0.95
16	0.16	35	27	1.61	0.49	0.73
17	0.23	35	26	1.17	0.34	0.67
18	0.16	35	26	1.70	0.49	0.84
19a	0.30	35	25	1.89	0.49	0.61
20	0.31	35	14	3.82	0.34	0.94
21	0.17	35	22	2.24	0.49	1.28

1 α determined by method 1 ($\theta = 35^{\circ}$)

2 α determined by method 2 ($\theta = \cos^{-1}(c/v_b)$)

3 ka determined from the upwave measurements

4 ka calculated from boat velocity

5 ka determined from the downwave measurements

Table 2: Summary of wave transmission data including the transmission coefficient, estimates of wave direction and ka for each test.

Test	kh	ka	H_d (cm)	H_u (cm)	K_t' uncorrected	C_t	K_t corrected
12	1.18	1.70	4.0	12.3	0.32	1.57	0.51
11	1.18	1.70	6.5	15.0	0.43	1.57	0.68
5	1.09	1.57	8.7	26.7	0.33	1.64	0.53
1	0.95	1.37	12.0	36.7	0.33	1.70	0.56
21	0.88	1.28	5.0	30.0	0.17	1.75	0.29
14	0.82	1.18	10.3	26.0	0.40	1.76	0.70
7	0.73	1.06	14.0	18.8	0.75	1.72	1.28
6	0.72	1.04	11.0	30.0	0.37	1.70	0.62
2	0.72	1.03	14.3	42.5	0.34	1.70	0.57
9	0.69	0.99	8.0	23.3	0.34	1.68	0.58
8	0.69	0.99	14.0	15.0	0.93	1.68	1.57
23	0.66	0.95	11.7	25.7	0.45	1.67	0.76
20	0.65	0.94	3.5	11.3	0.31	1.66	0.51
26	0.61	0.89	12.3	23.0	0.54	1.63	0.87
18	0.58	0.84	7.0	43.3	0.16	1.57	0.25
16	0.51	0.73	6.0	36.7	0.16	1.42	0.23
24	0.47	0.69	19.3	25.0	0.77	1.36	1.05
25	0.47	0.68	6.5	45.0	0.14	1.36	0.20
17	0.47	0.67	5.7	25.0	0.23	1.34	0.30
19a	0.42	0.61	6.3	21.0	0.30	1.27	0.38
10	0.42	0.61	16.3	21.0	0.78	1.27	0.99

Table 3: Corrected and uncorrected field results.

	Case 1	Case 2
Width	3.963 m	3.963 m
Height	0.915 m	1.728 m
Draft	0.559 m	1.372 m
Area	3.626 m^2	6.848 m^2
Submerged Area	2.215 m^2	5.437 m^2
Moment of Inertia	0.253 m^4	1.704 m^4
Radius of Gyration	0.264 m	0.499 m
Centroid of Waterplane Area	0.000 m	0.000 m
Centre of Gravity	-0.102 m	-0.102 m
Centre of Buoyancy	-0.280 m	-0.280 m

Table 4: Breakwater characteristics used in the numerical model.

Photographs

Figures

Type *View*

Box

Solid Rectangle

Barge

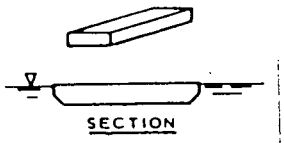

Pontoon

Twin Pontoon

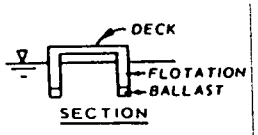

Open Compartment

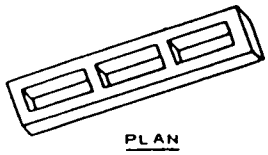

A Frame

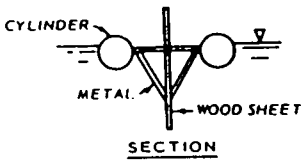

Twin Log

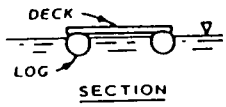

Mat

Tire Mat

Log Mat

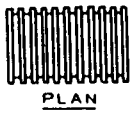

Tethered Float

Sphere

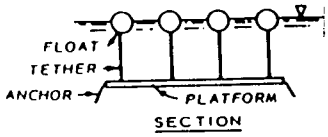

Tire

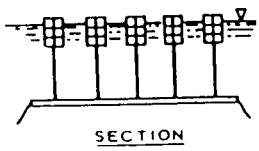

Figure 1: Types and configurations of floating breakwater designs (after McCartney, 1985).

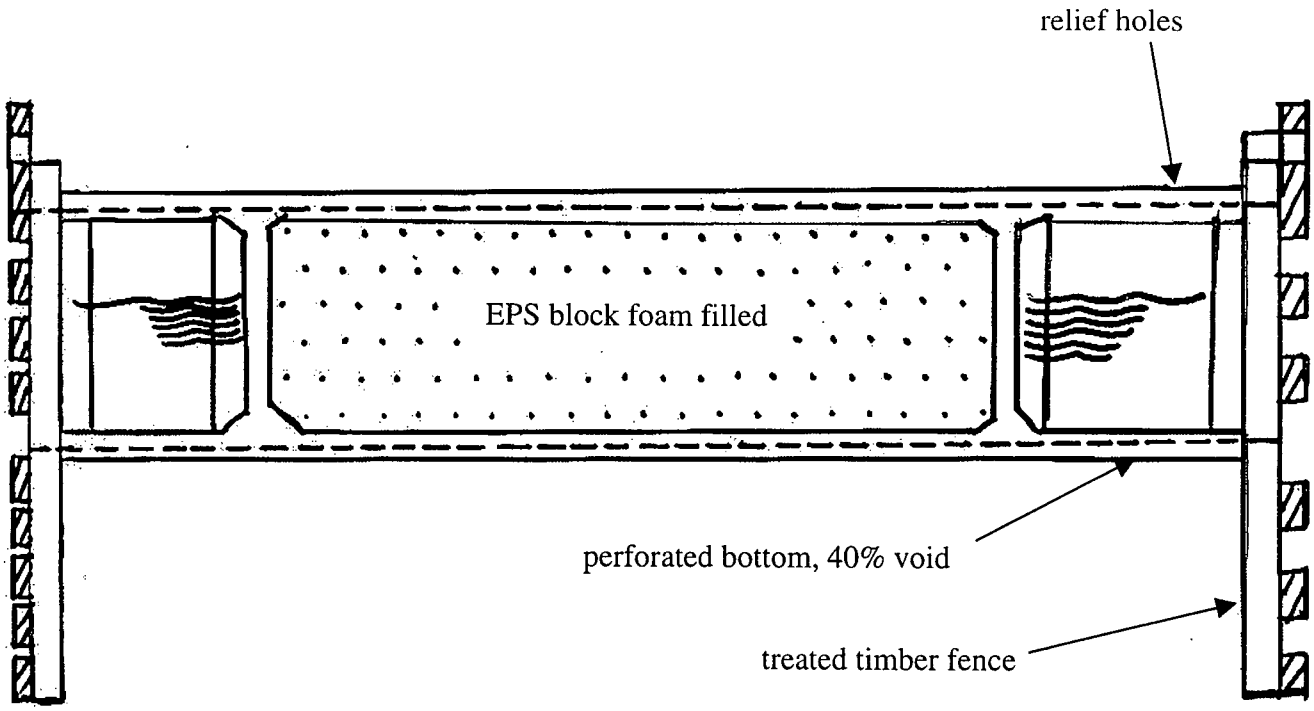

Figure 2: Cross-section of the Saltspring floating breakwater (after CeFer Floating Structures, Inc., 1997).

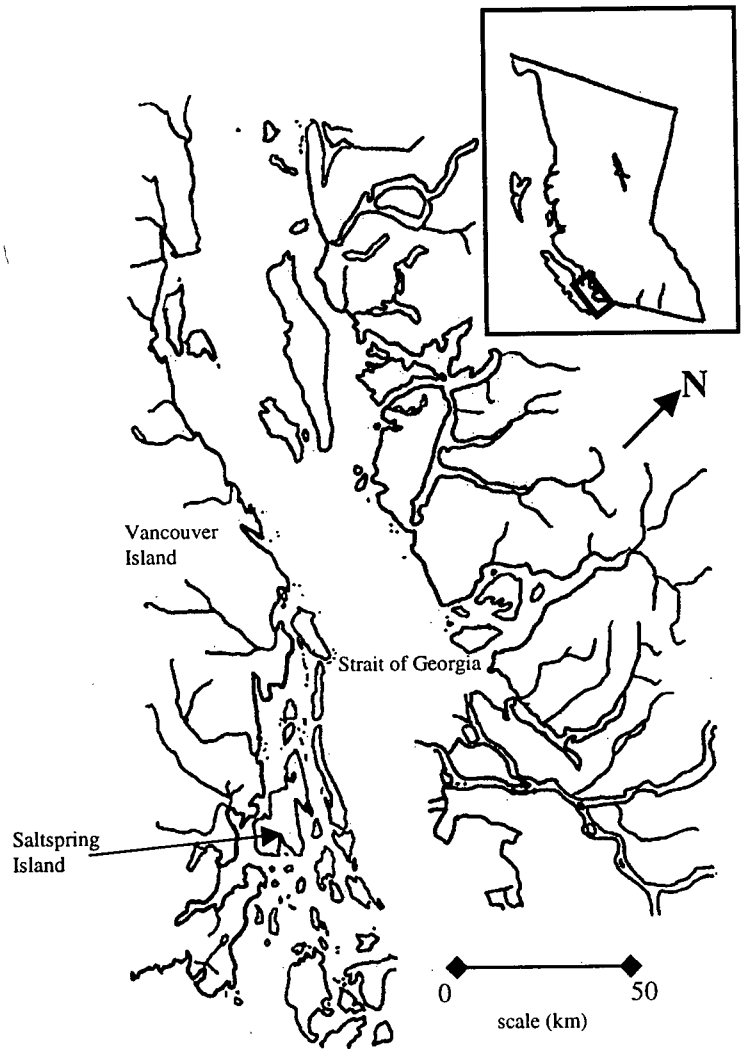

Figure 3: Map of British Columbia showing the location of Saltspring Island (after Byres, 1988).

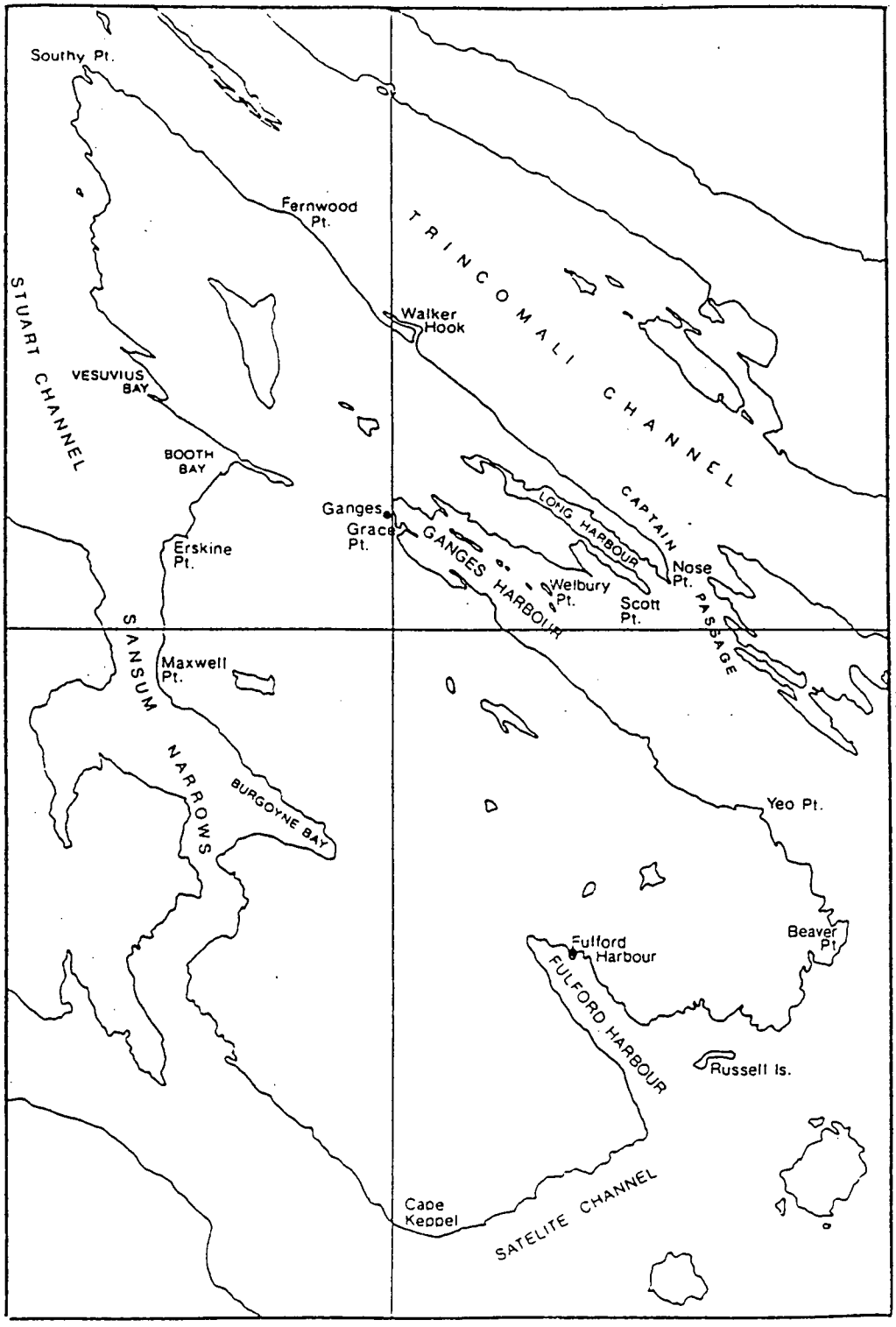

Figure 4: Map of Saltspring Island showing the location of Ganges (after Owens, 1980).

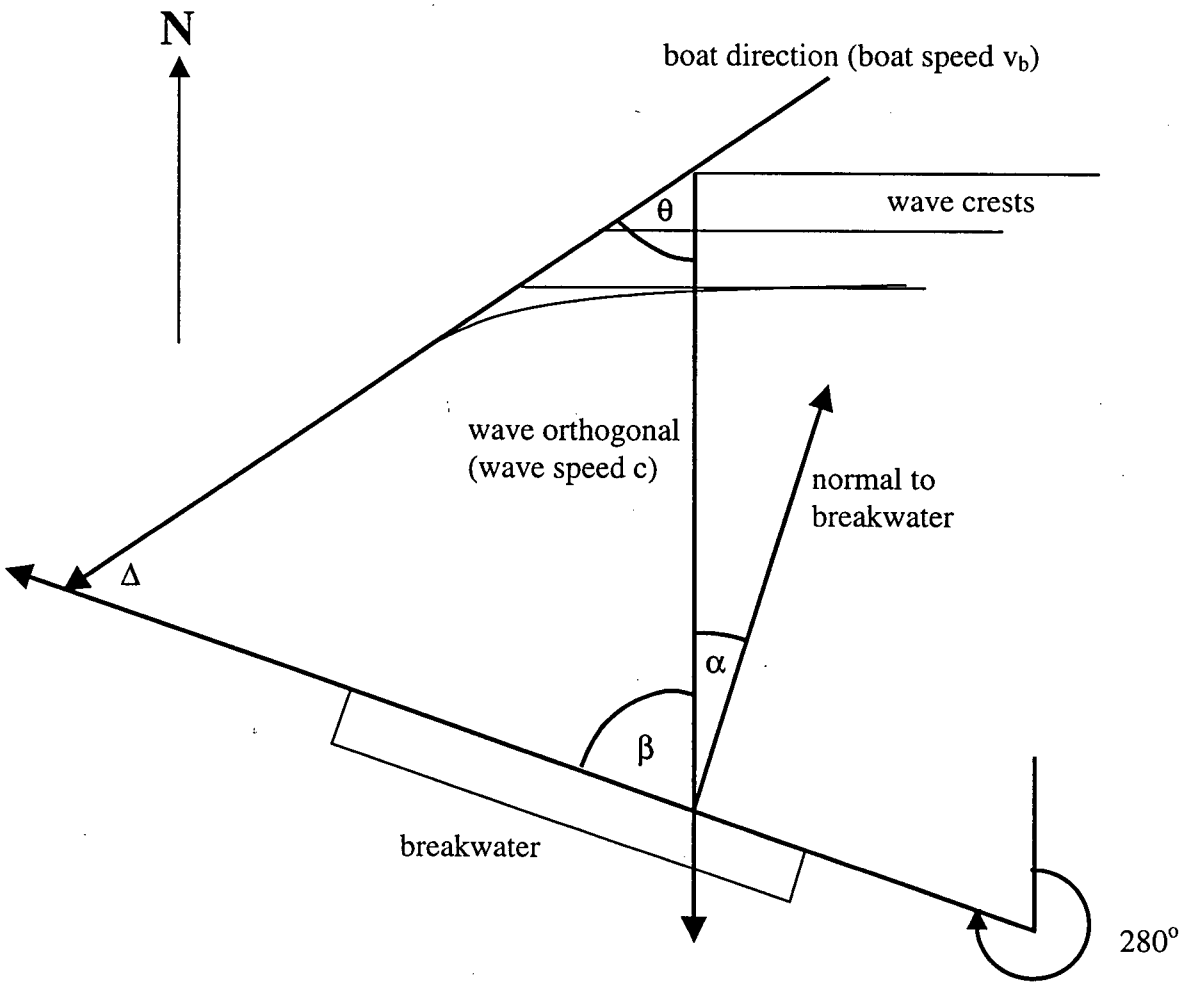

Figure 5: Definition sketch of wave direction relative to boat direction and breakwater location.

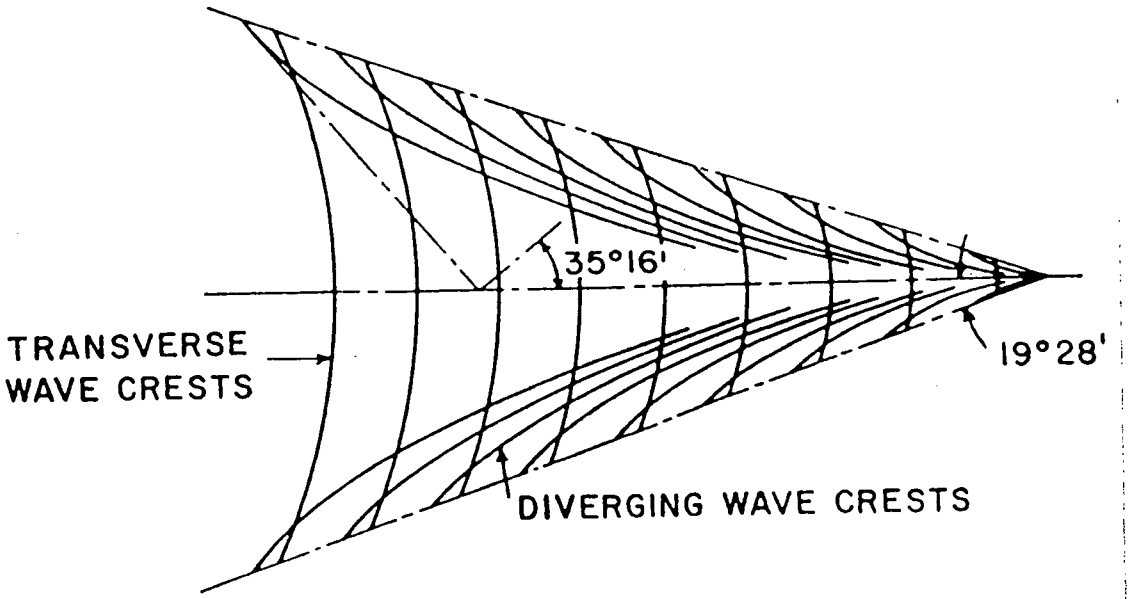

Figure 6: The Kelvin ship-wave pattern (after Newman, 1977), showing diverging wave crests which change in direction along the crests.

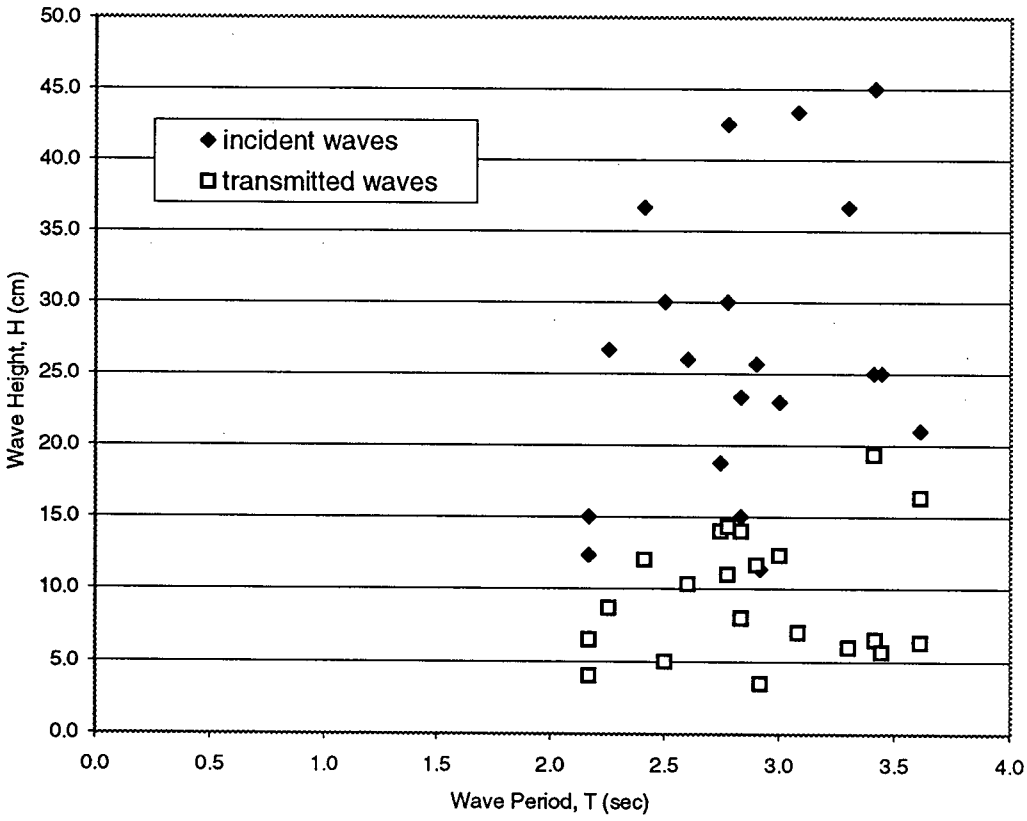

Figure 7: Field test results: Incident and transmitted wave heights for various wave periods.

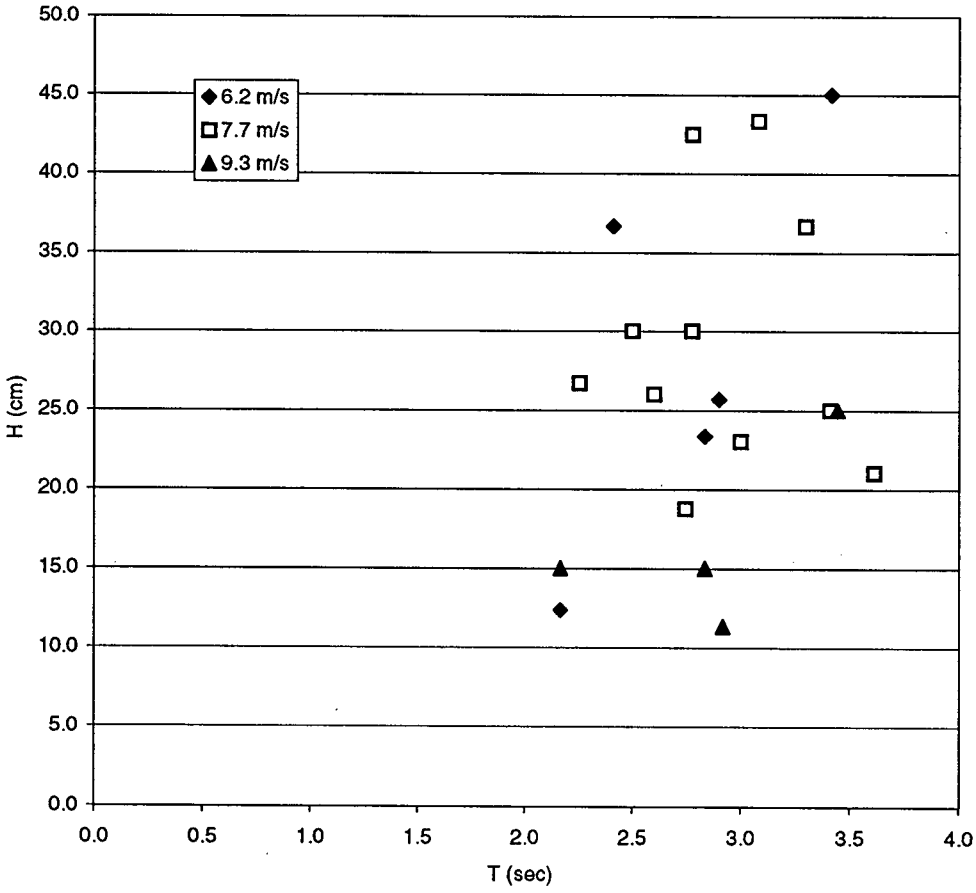

Figure 8: Incident wave height and wave period for various boat speeds.

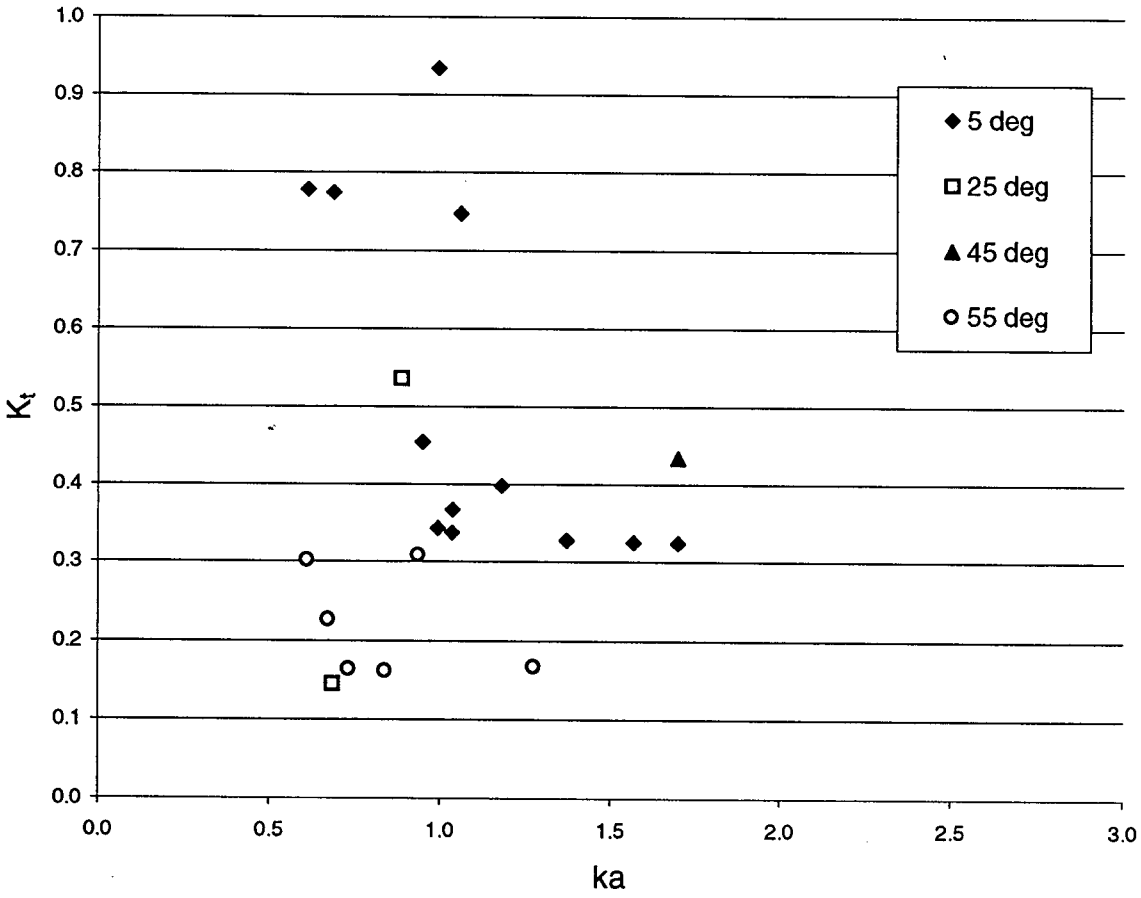

Figure 9: Field test results: transmission coefficient as a function of ka for various wave directions.

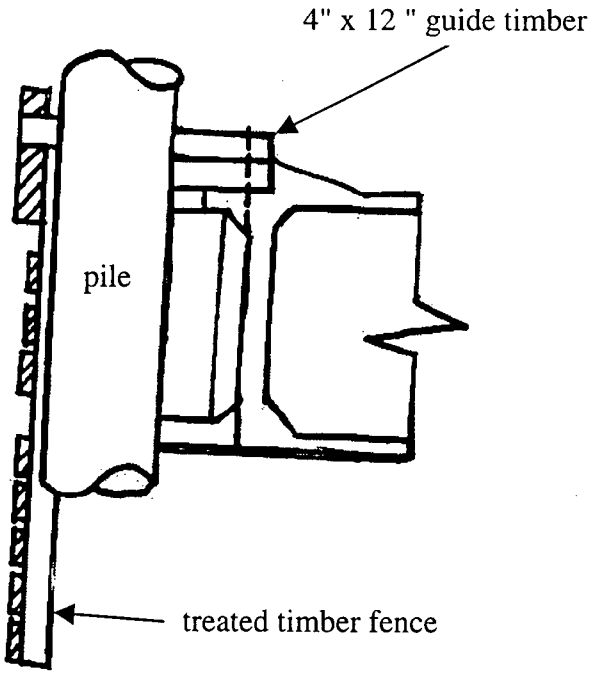

Figure 10: Cross-section of a pile well (after CeFer Floating Structures, Inc., 1997).

a)

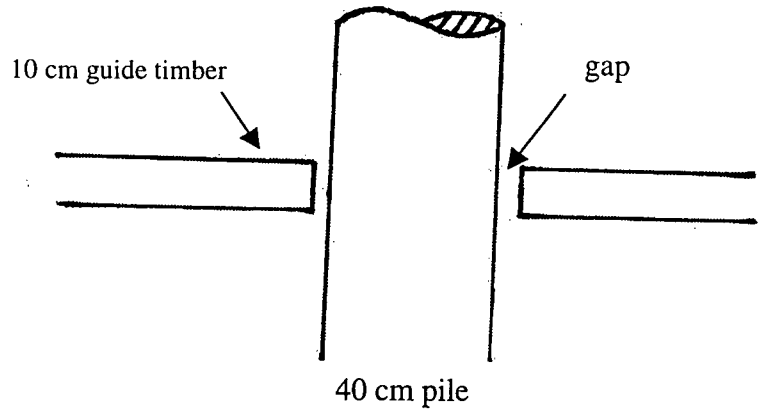

b)

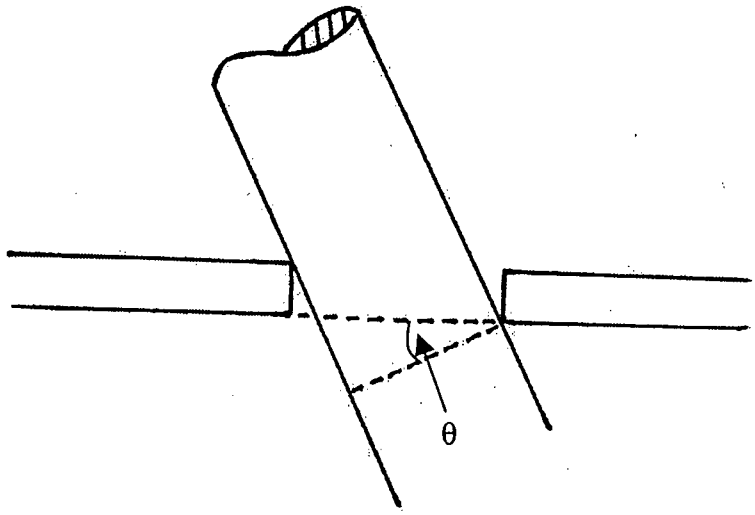

Figure 11: Sketch showing a) the gap between the pile and guide timbers and b) the maximum allowable roll angle θ for a given gap width (note the corners of the guide timbers where crushing would occur resulting in even greater roll).

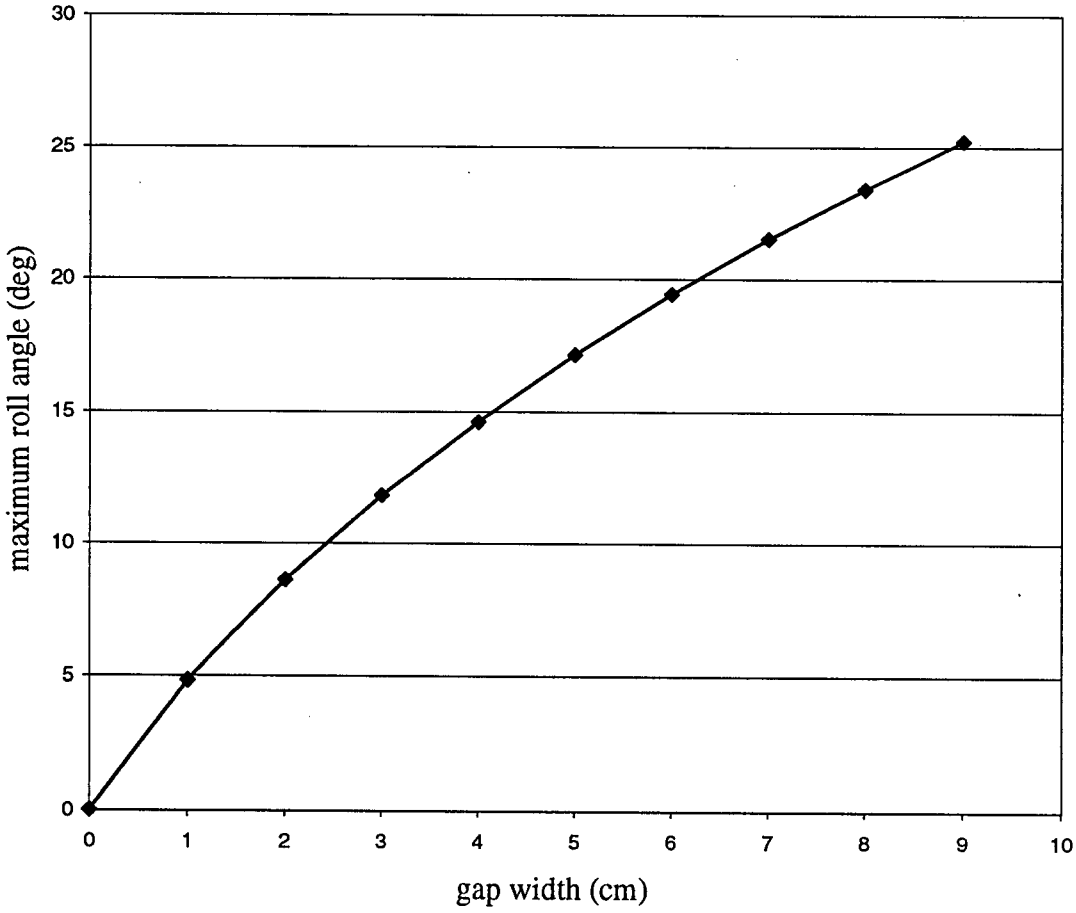

Figure 12: Predicted allowable maximum roll angles for varying gap widths.

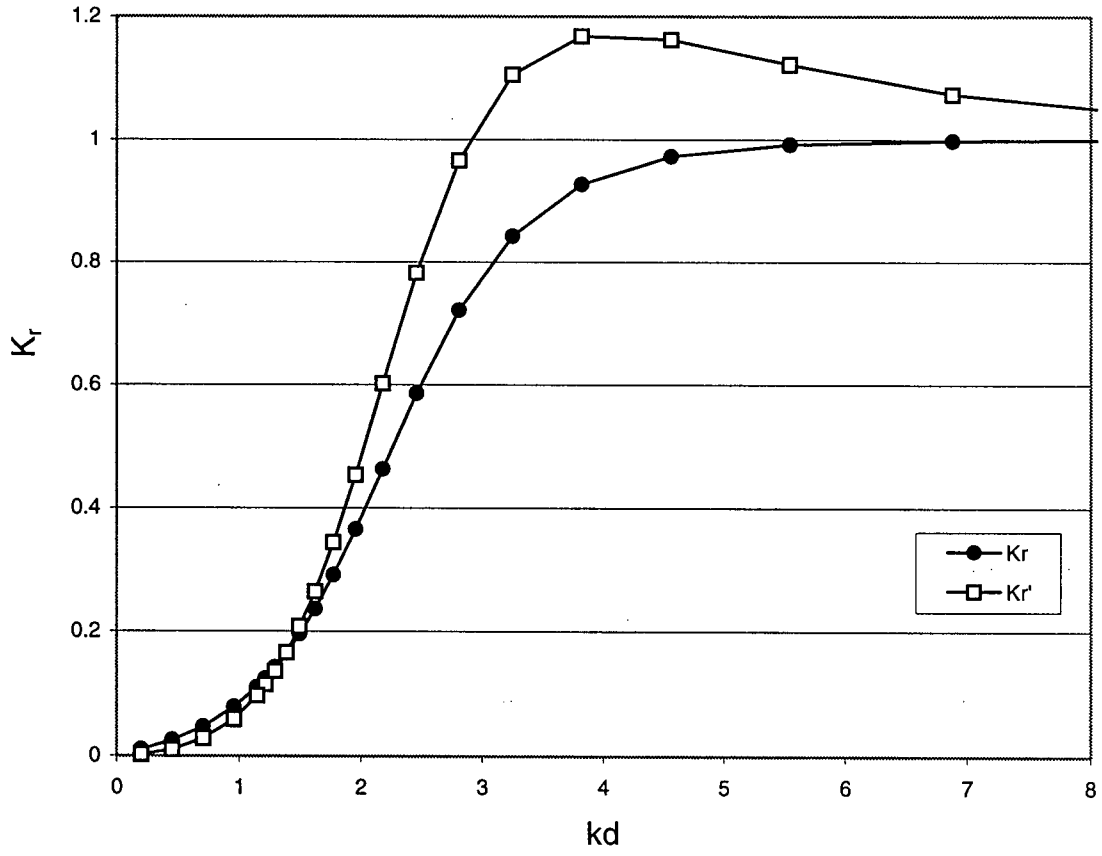

Figure 13: Reflection coefficient as a function of kd for a solid barrier, estimated close to and far from the barrier.

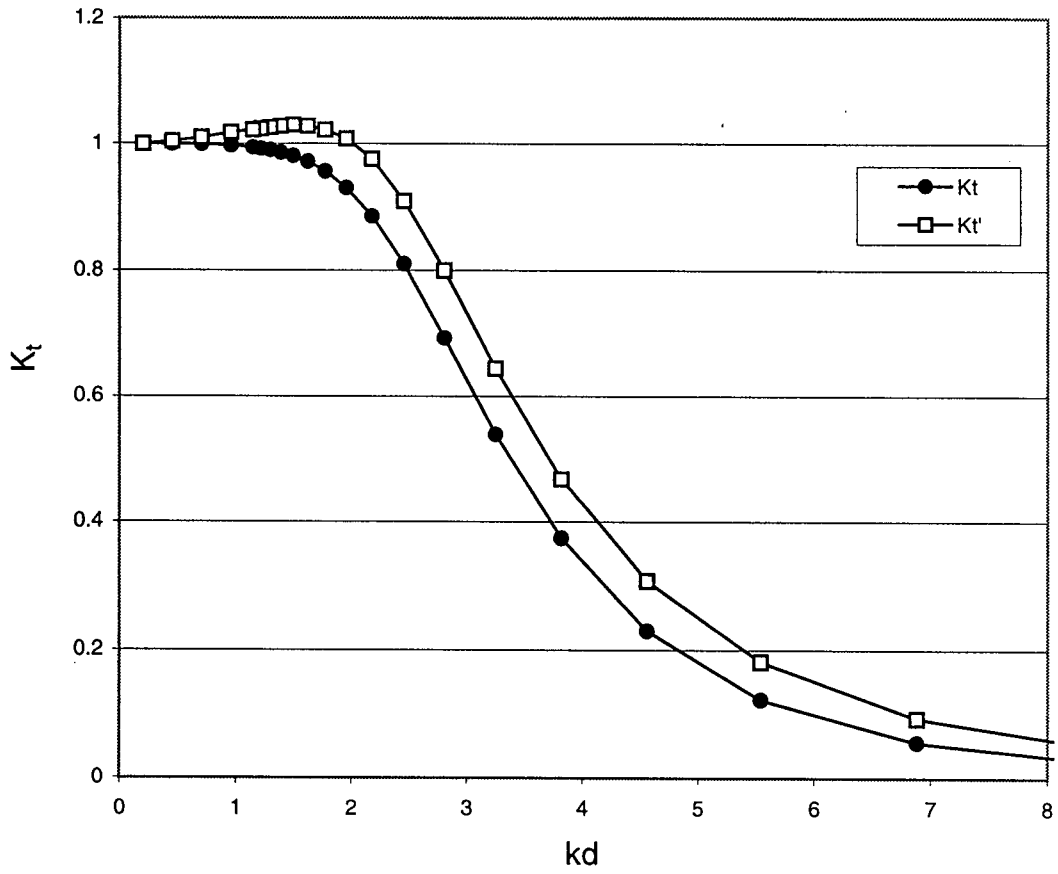

Figure 14: Transmission coefficient as a function of kd for a solid barrier, estimated close to and far from the barrier.

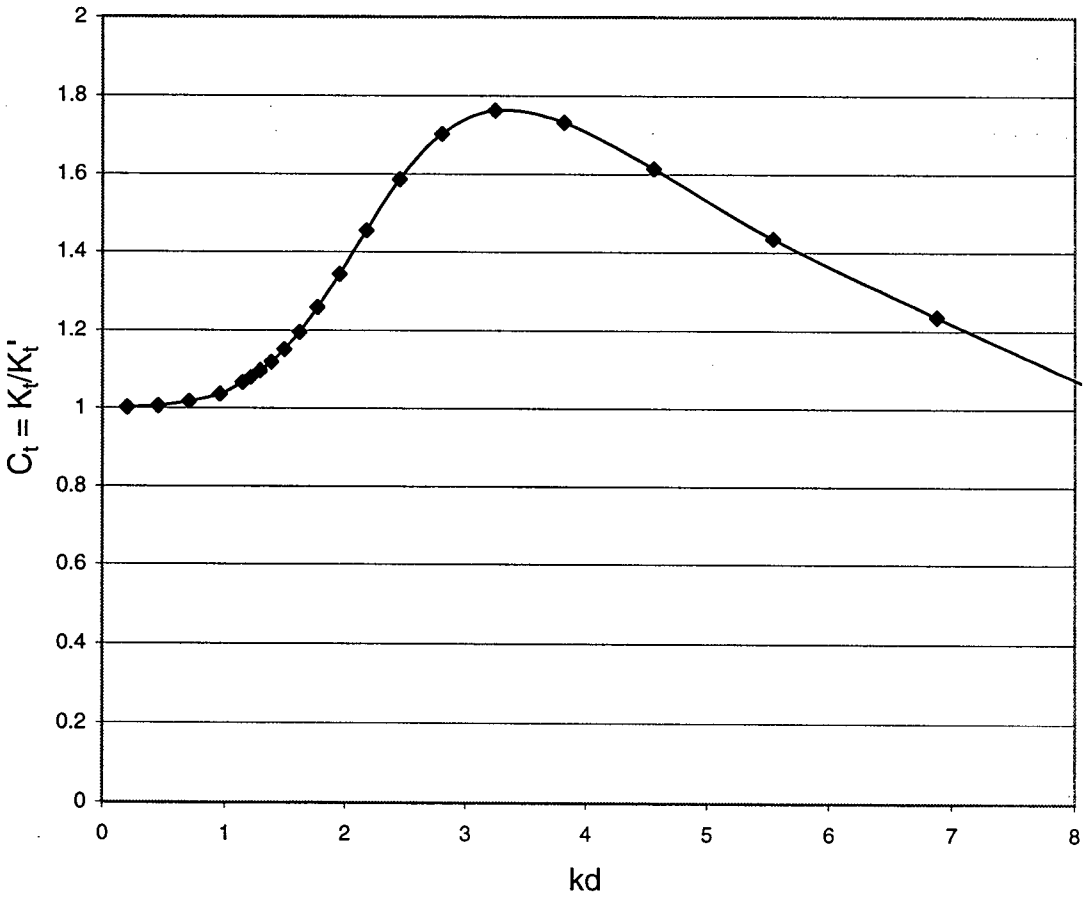

Figure 15: Wave transmission correction factor as a function of kd.

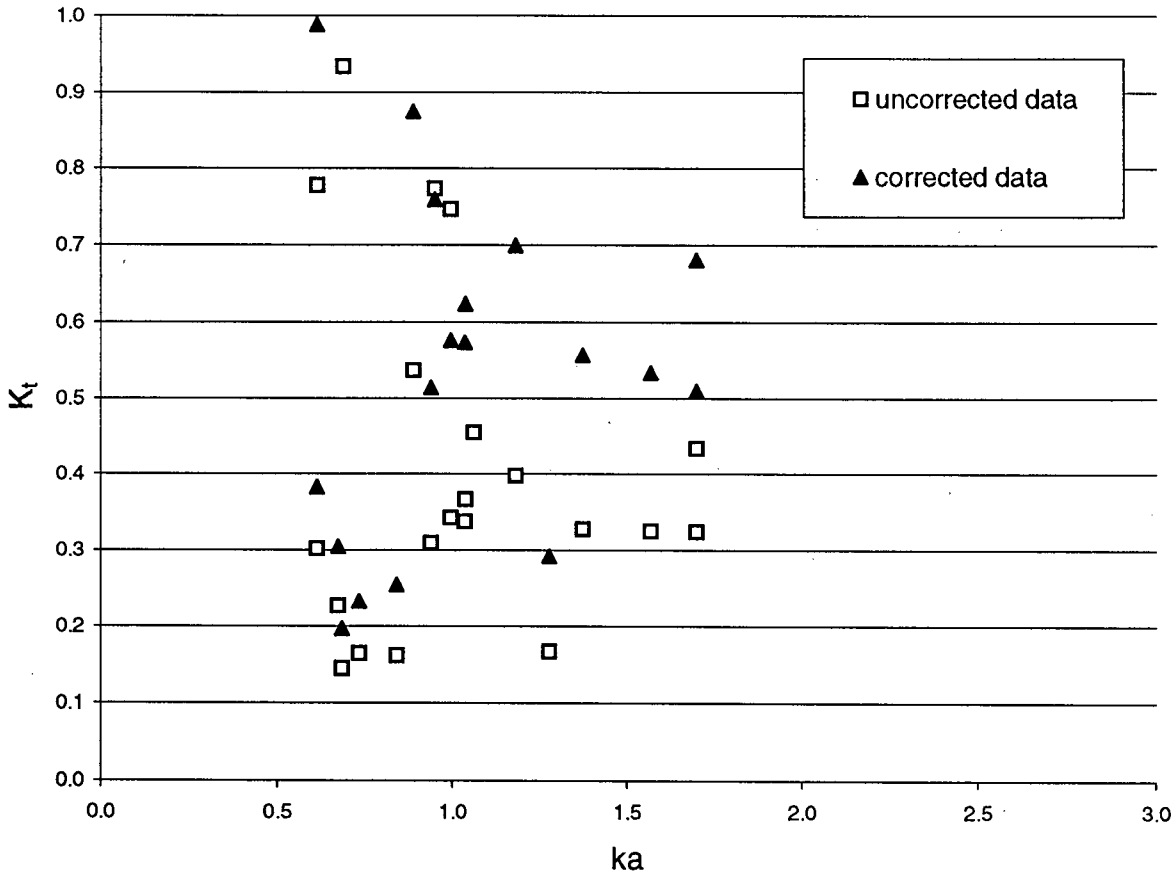

Figure 16: Field test results: transmission coefficient as a function of ka for corrected and uncorrected data.

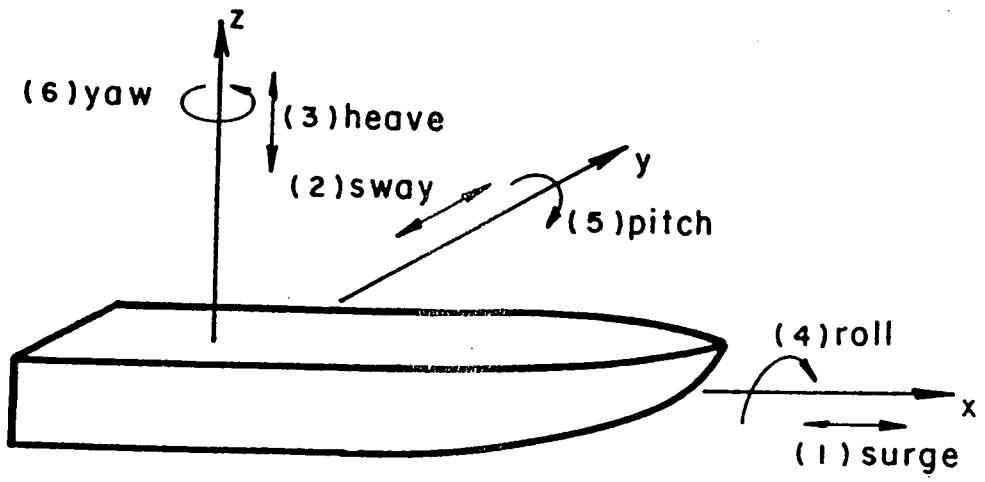

Figure 17: Definition sketch of floating breakwater motions (after Sarpkaya and Isaacson, 1981).

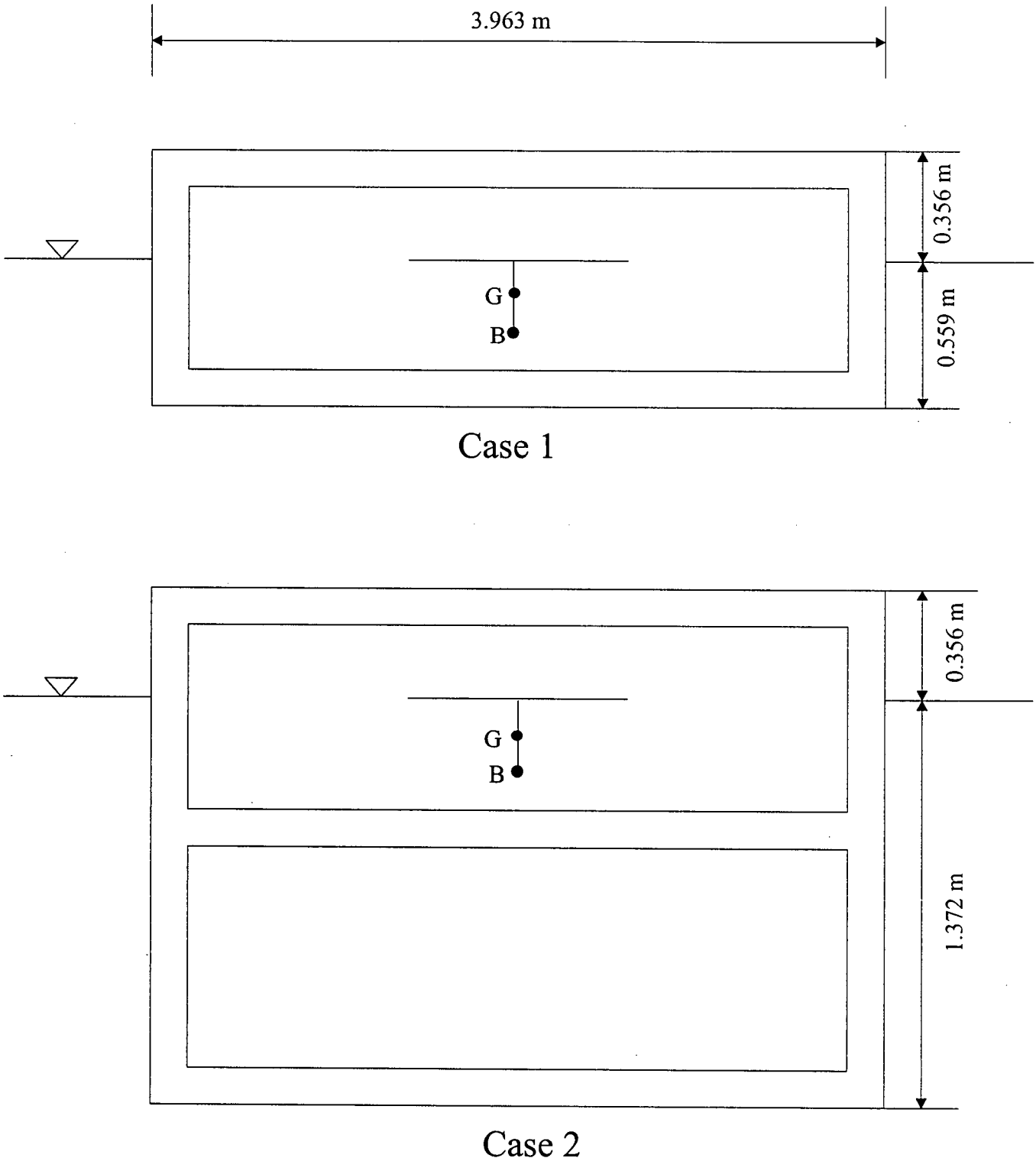

Figure 18: Sketch of two cases of idealized breakwater dimensions.

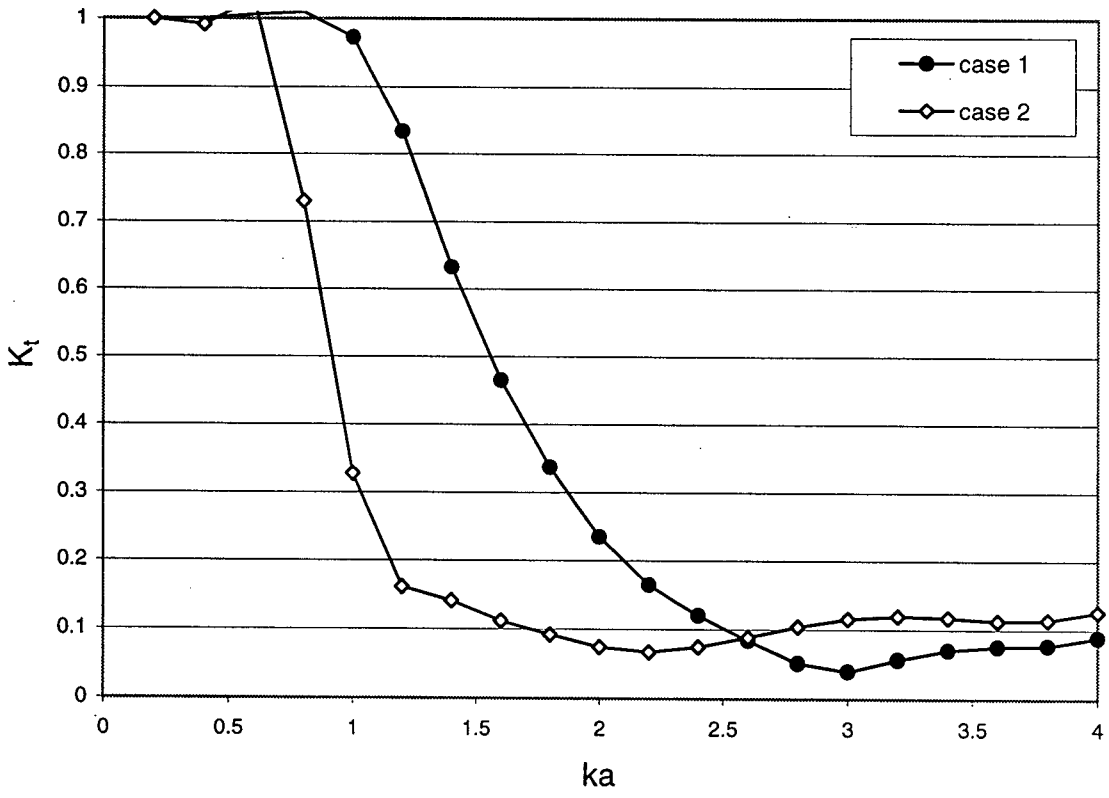

Figure 19: Transmission coefficient as a function of ka for two cases of breakwater dimensions ($\zeta = 0\%$, $\alpha = 0^{\circ}$, dof = heave-only).

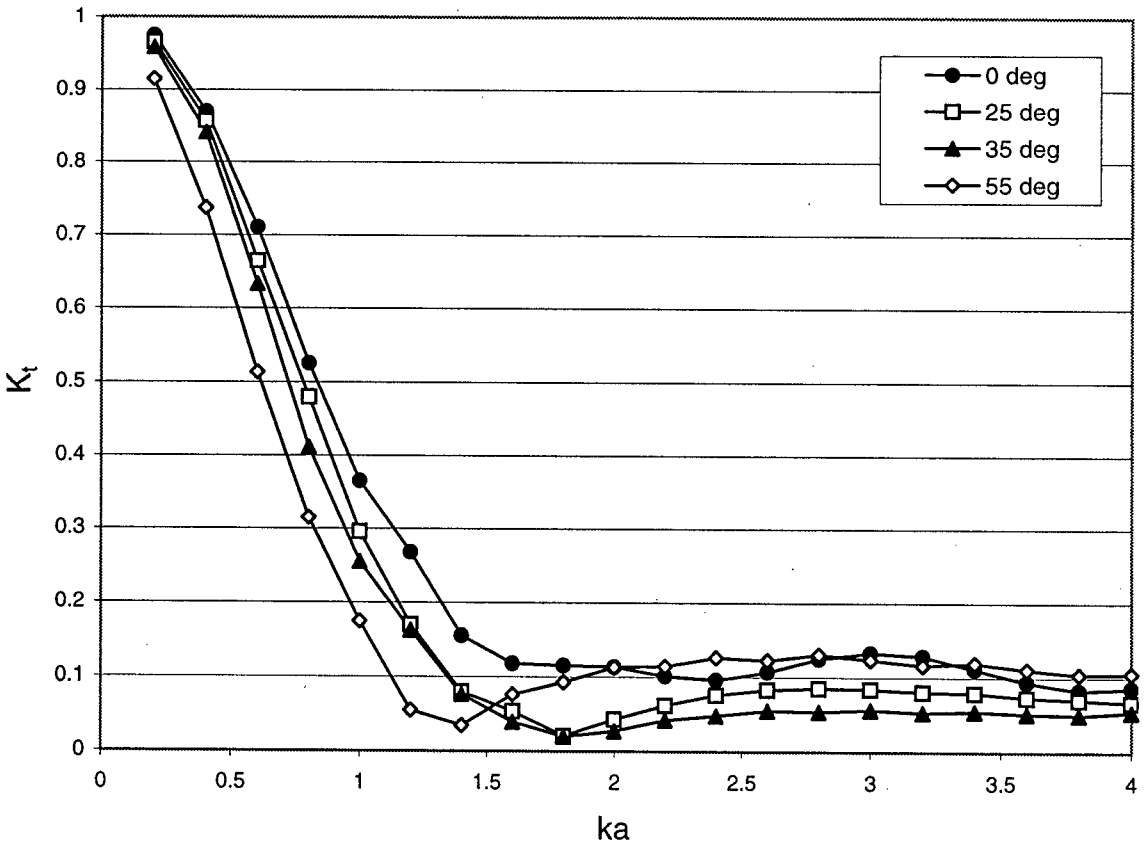

Figure 20: Transmission coefficient as a function of ka for various incident wave directions (ζ = 0%, case = 1, dof = fixed).

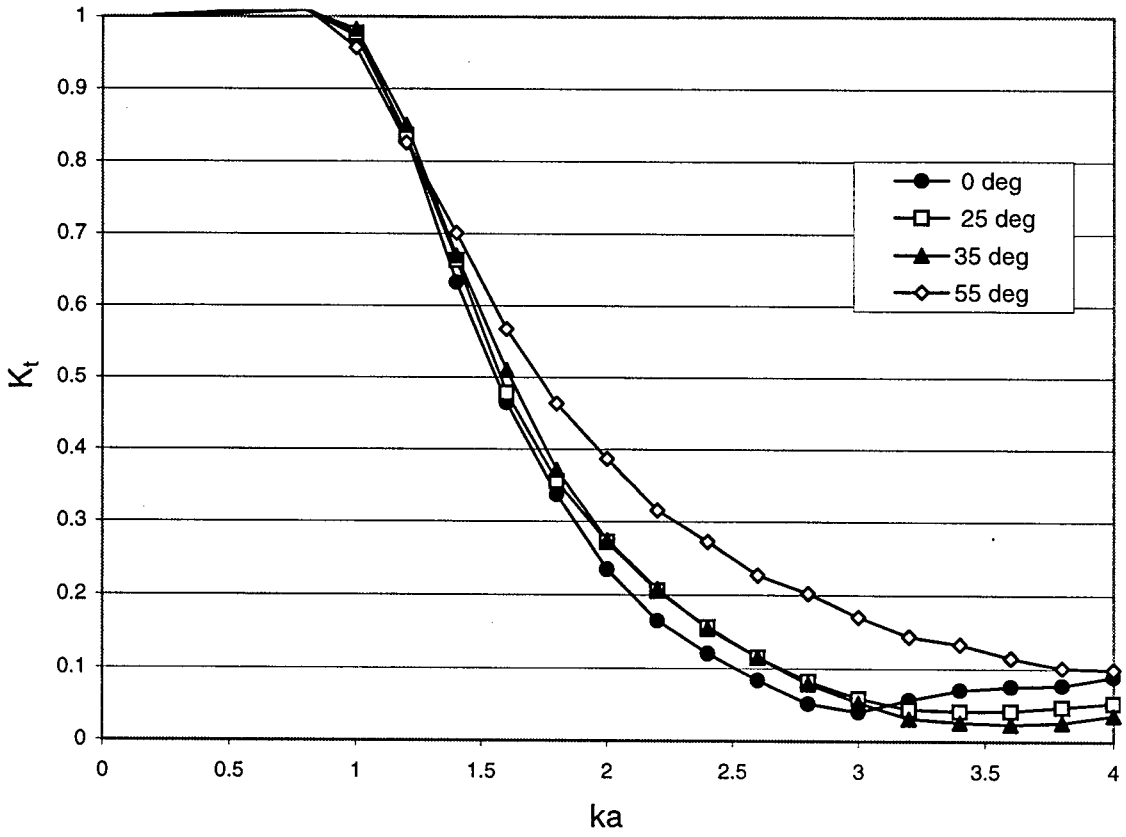

Figure 21: Transmission coefficient as a function of ka for various incident wave directions (ζ = 0%, case = 1, dof = heave-only).

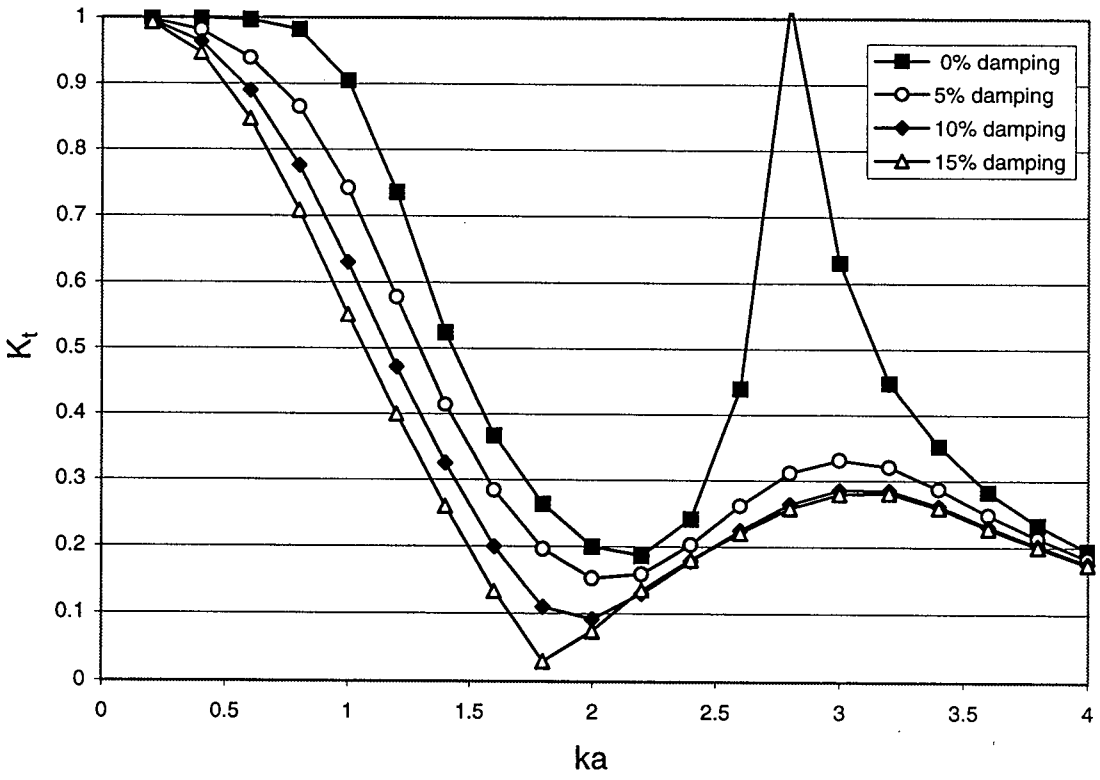

Figure 22: Transmission coefficient as a function of ka for various damping coefficients (case = 1, dof = freely floating, $\alpha = 0^{o}$).

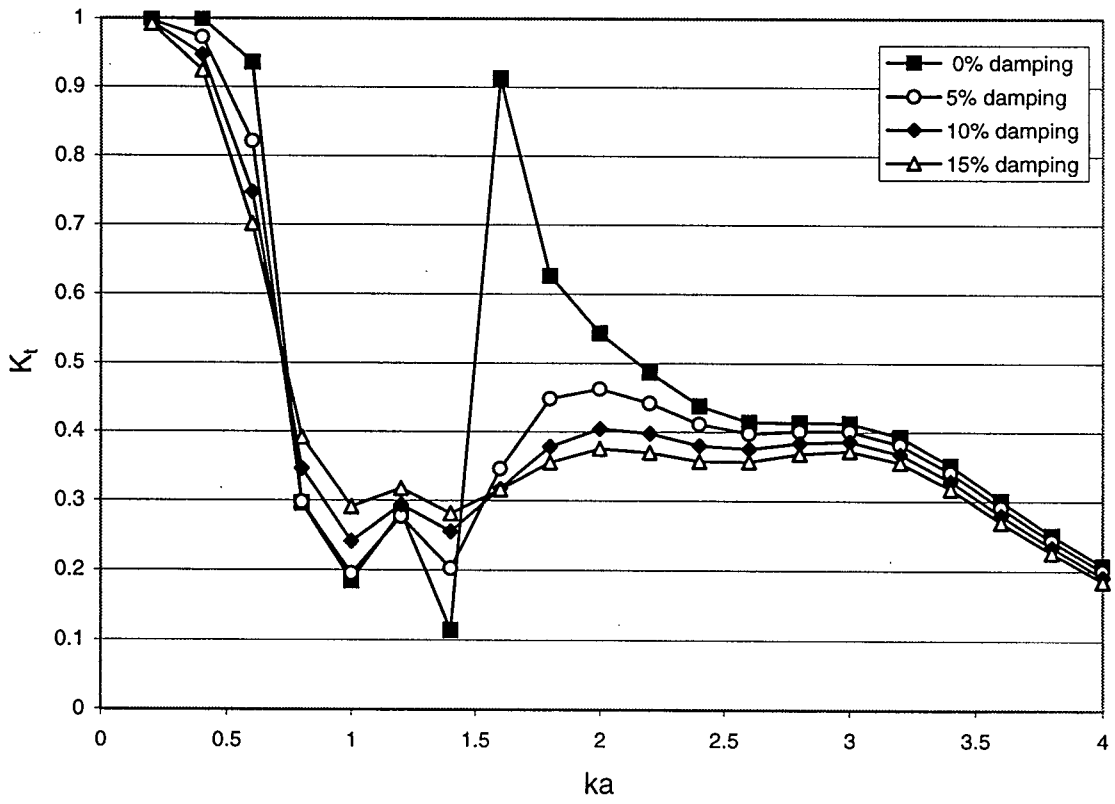

Figure 23: Transmission coefficient as a function of ka for various damping coefficients (case = 2, dof = freely floating, $\alpha = 0^{o}$).

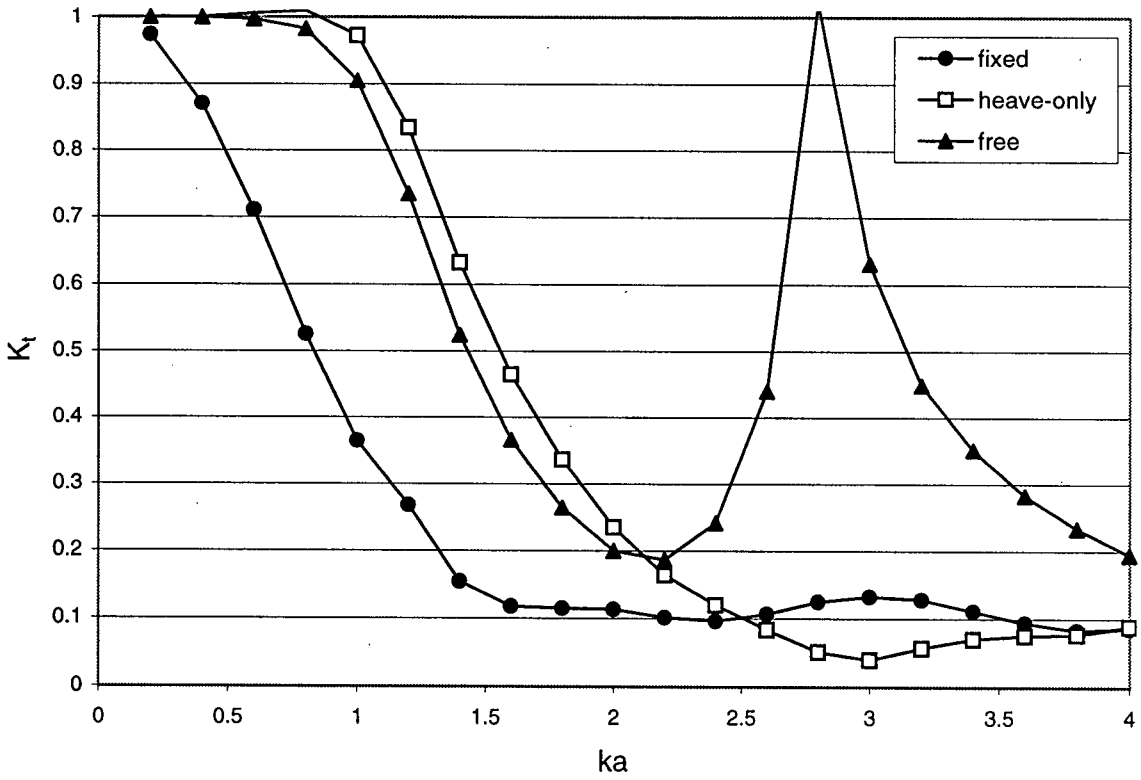

Figure 24: Transmission coefficient as a function of ka for various breakwater motions ($\zeta = 0\%$, case = 1, $\alpha = 0^{o}$).

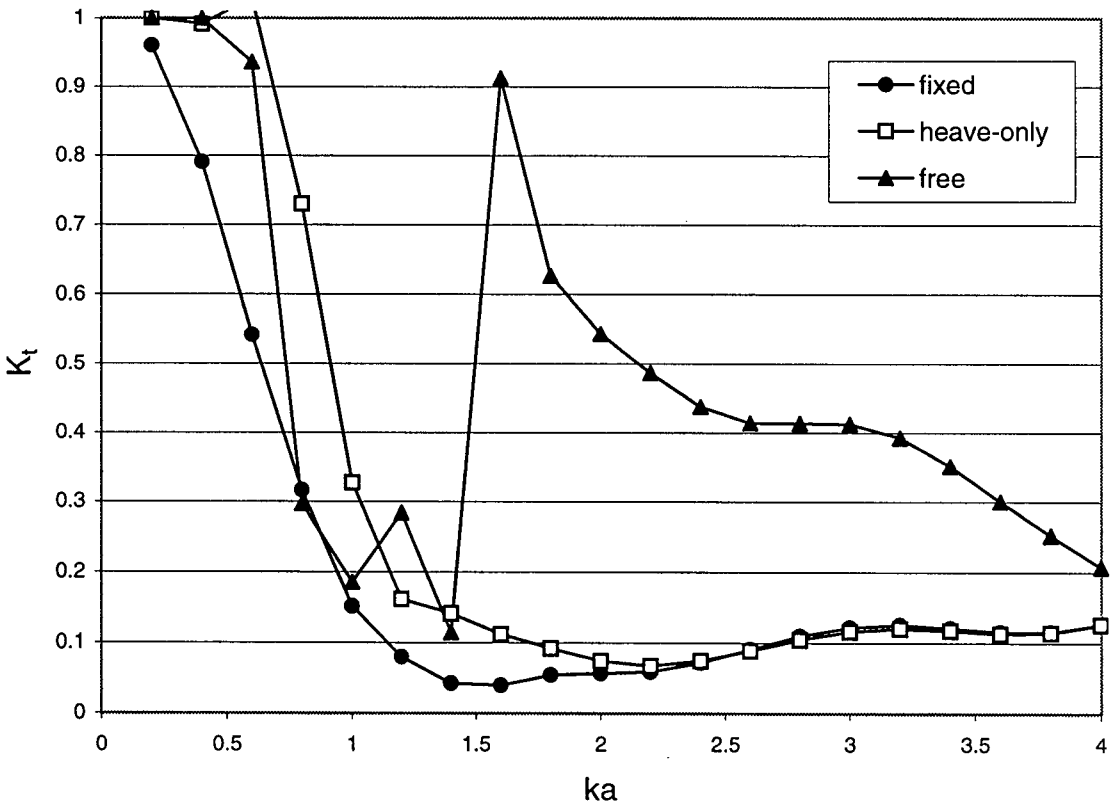

Figure 25: Transmission coefficient as a function of ka for various breakwater motions ($\zeta = 0\%$, case = 2, $\alpha = 0^{o}$).

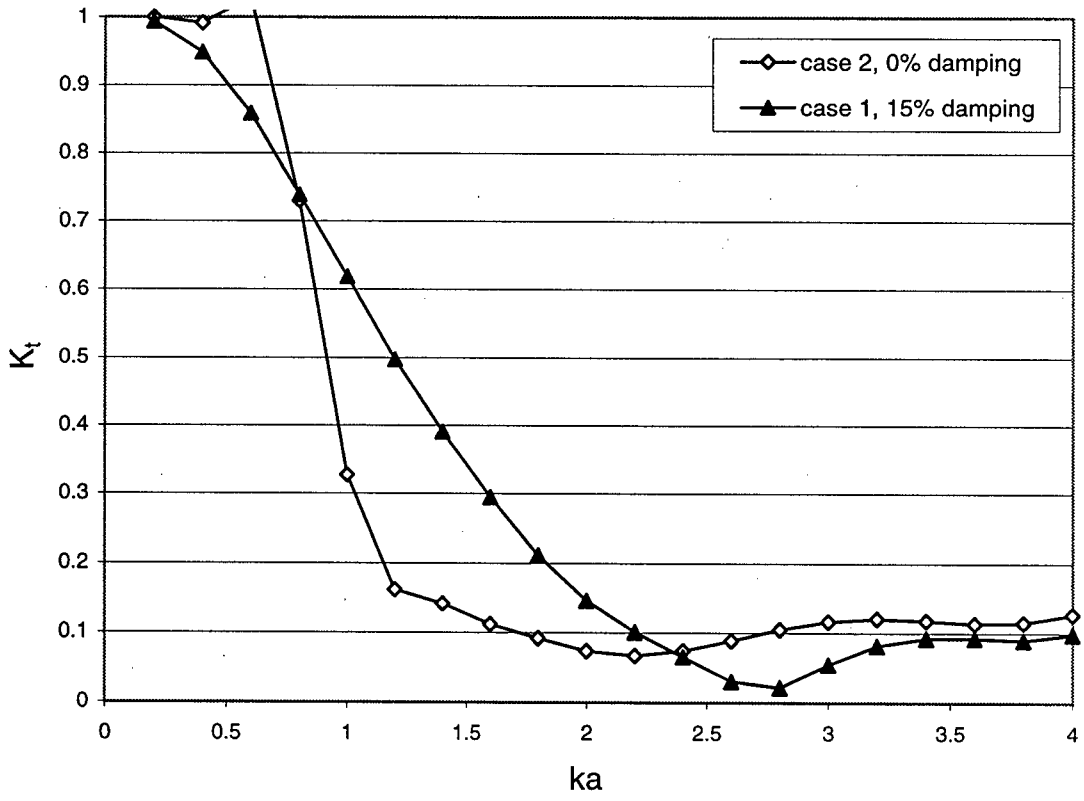

Figure 26: Transmission coefficient as a function of ka for damped case 1 and undamped case 2 ($\alpha = 0^{o}$, dof = heave-only).

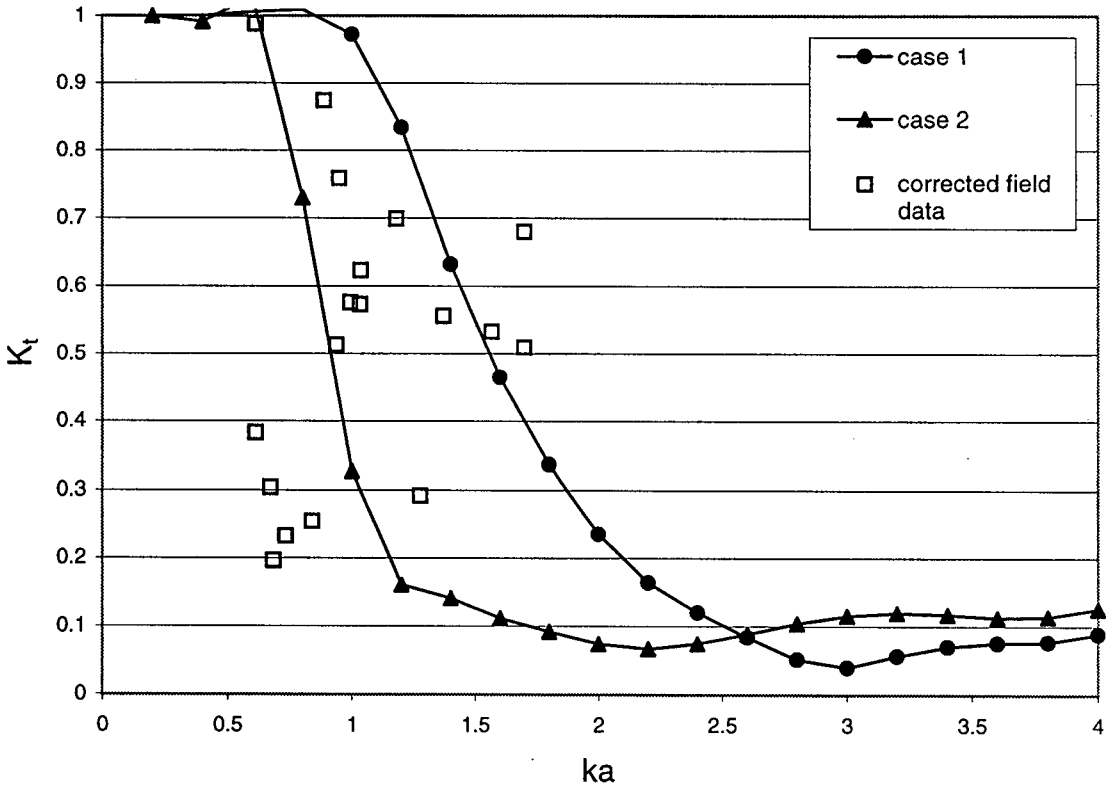

Figure 27: Comparison of field data and numerical results: transmission coefficient as a function of ka for two cases of breakwater dimensions ($\zeta = 0\%$, $\alpha = 0^{o}$, dof = heave-only).

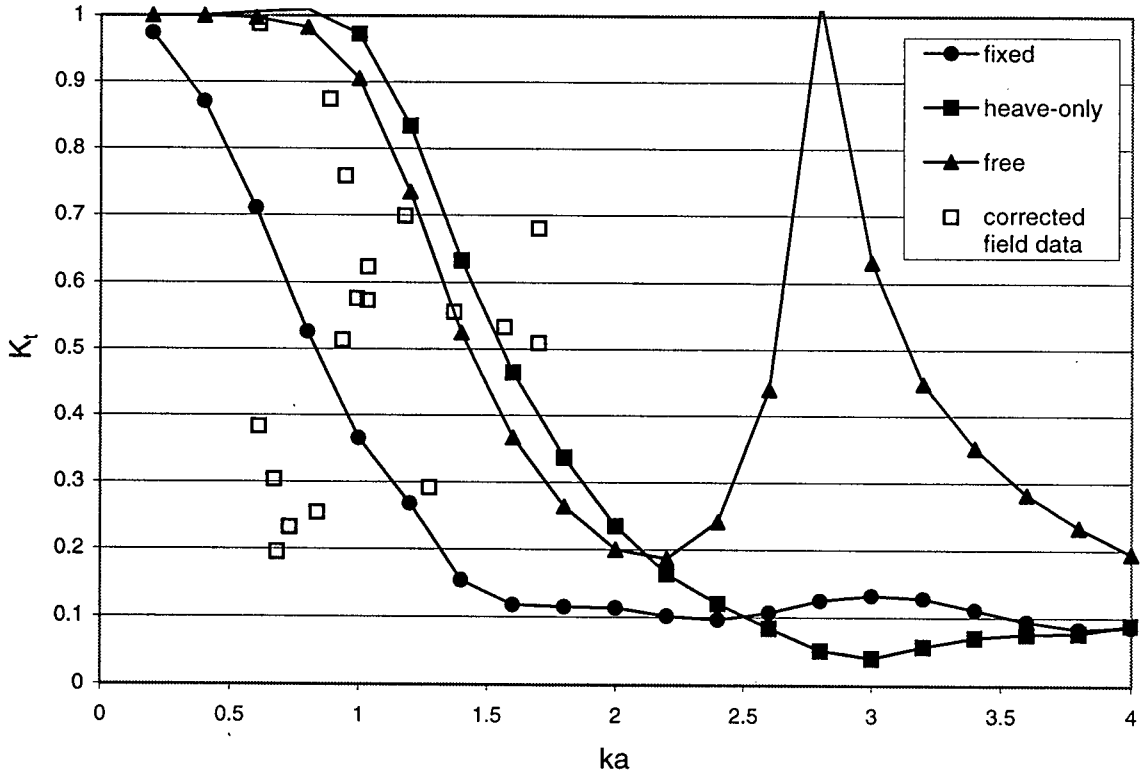

Figure 28: Comparison of field data and numerical results: transmission coefficient as a function of ka for various breakwater motions ($\zeta = 0\%$, case = 1, $\alpha = 0^{o}$).

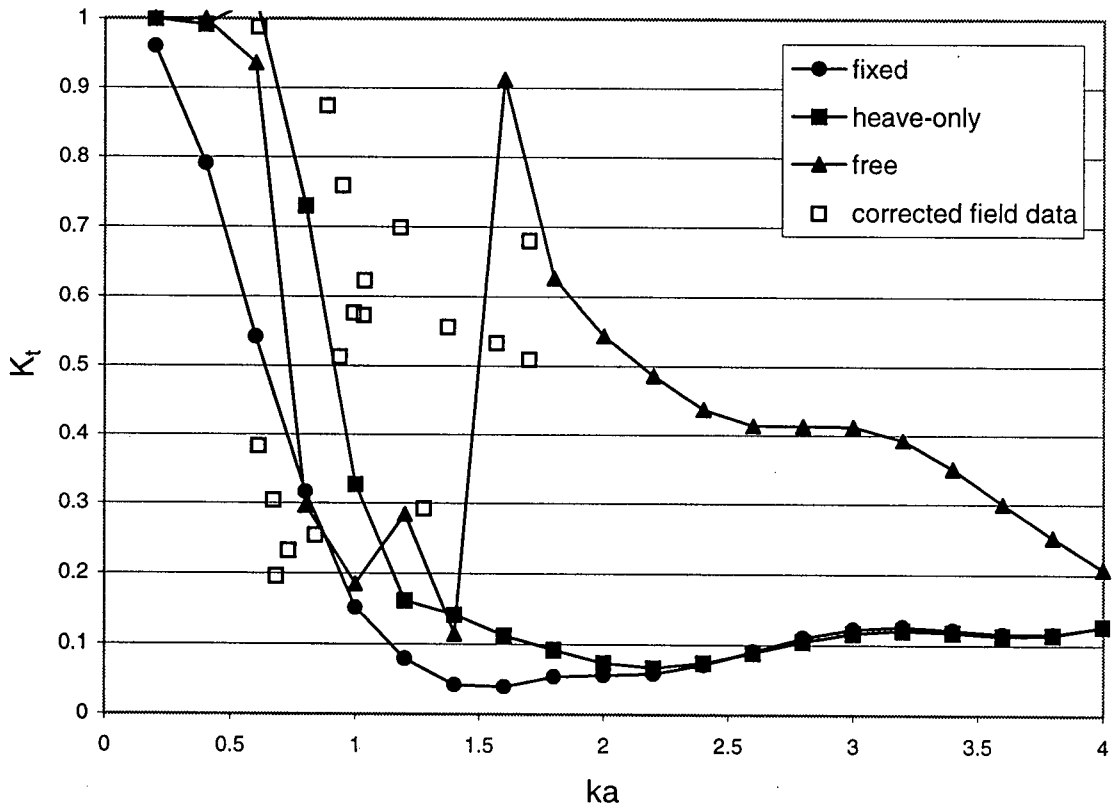

Figure 29: Comparison of field data and numerical results: transmission coefficient as a function of ka for various breakwater motions ($\zeta = 0\%$, case = 2, $\alpha = 0^{o}$).

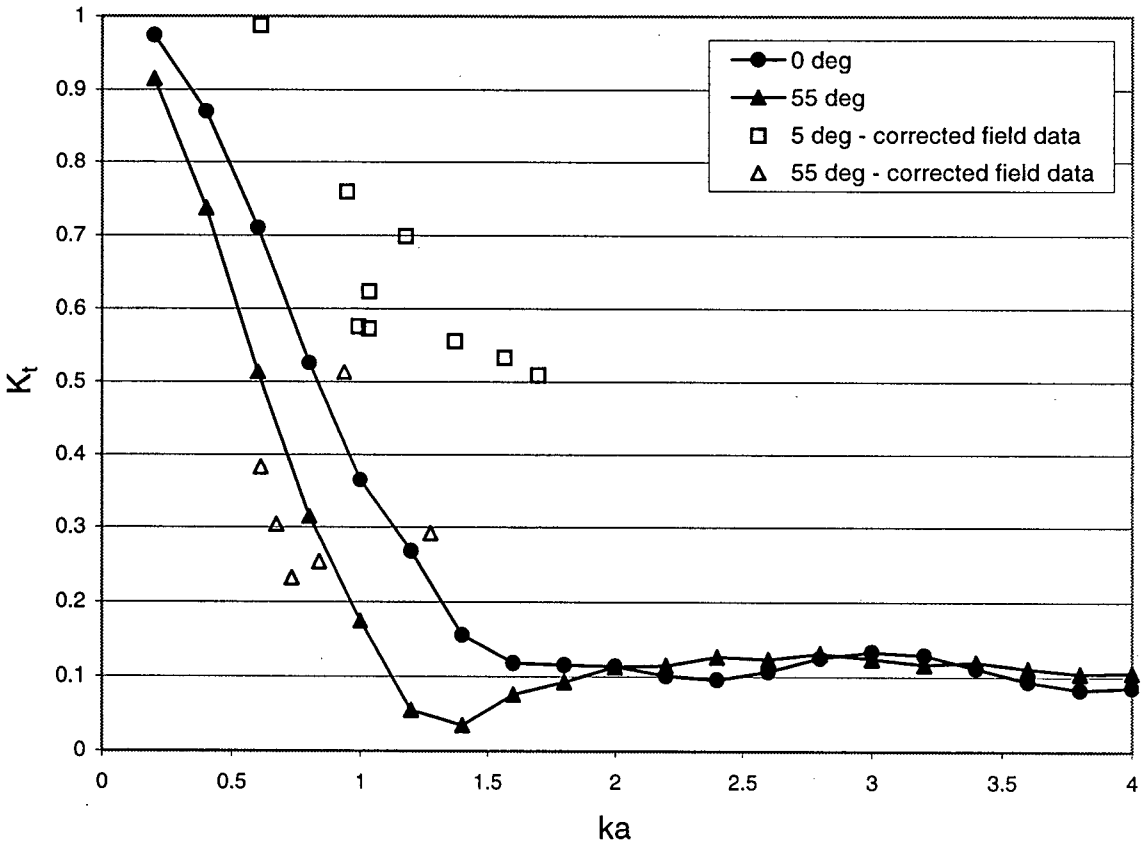

Figure 30: Comparison of field data and numerical results: transmission coefficient as a function of ka for various incident wave directions (ζ = 0%, case = 1, dof = fixed).

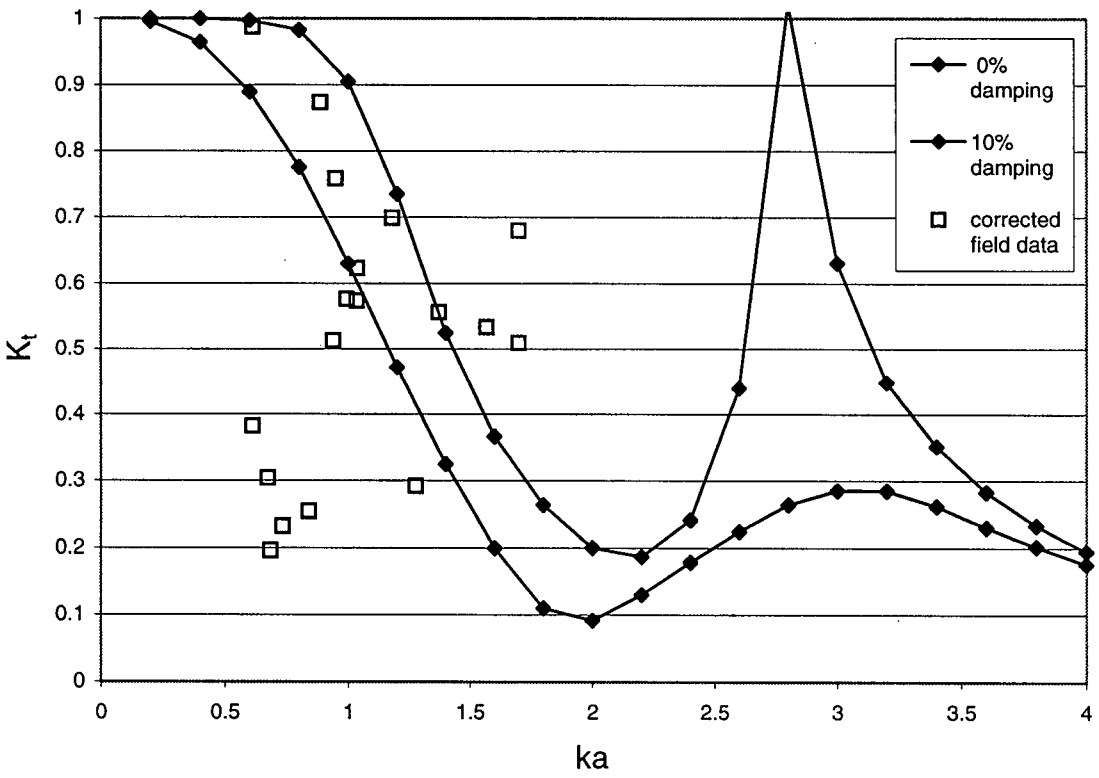

Figure 31: Comparison of field data and numerical results: transmission coefficient as a function of ka for various damping coefficients (case = 1, dof = freely floating, $\alpha = 0^{o}$).

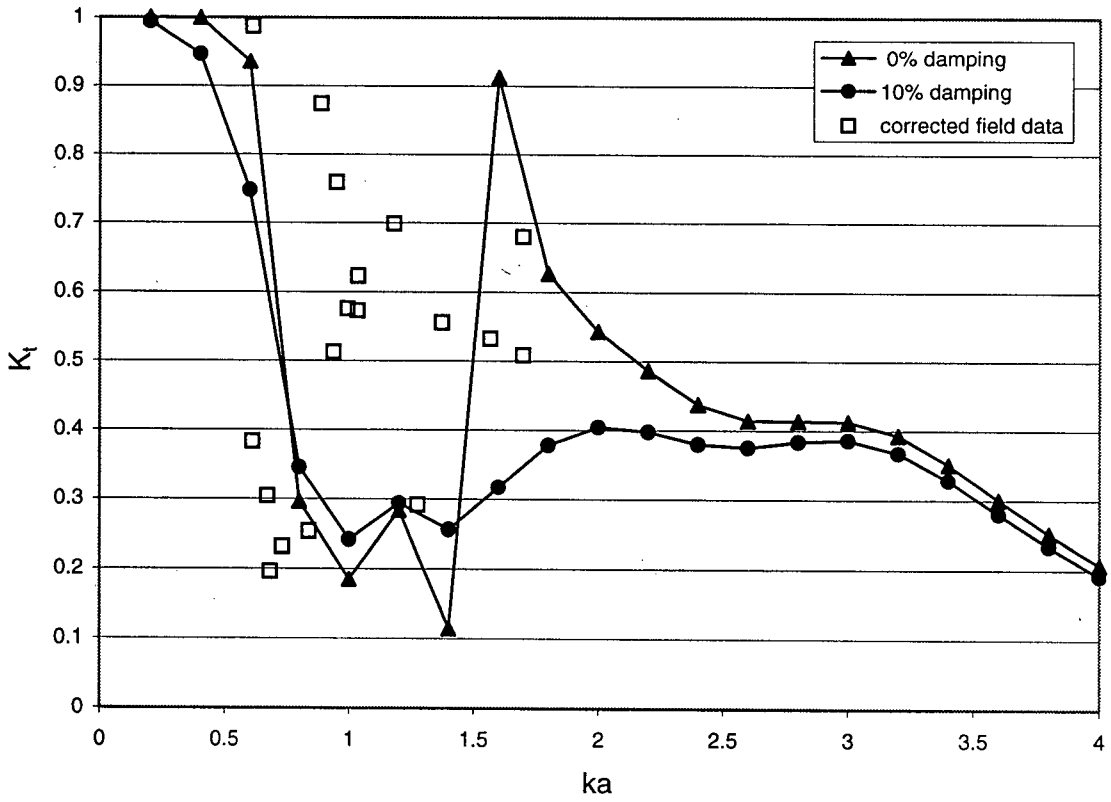

Figure 32: Comparison of field data and numerical results: transmission coefficient as a function of ka for various damping coefficients (case = 2, dof = freely floating, $\alpha = 0^{o}$).